

LA-NUREG-6713

C3

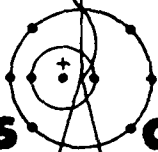
CIC-14 REPORT COLLECTION  
**REPRODUCTION  
COPY**

NRC-3

**Decay Heat from Products of  $^{235}\text{U}$  Thermal Fission  
by Fast-Response Boil-Off Calorimetry**



Issued: September 1977



**los alamos**  
**scientific laboratory**  
of the University of California  
LOS ALAMOS, NEW MEXICO 87545

An Affirmative Action/Equal Opportunity Employer

UNITED STATES  
ENERGY RESEARCH AND DEVELOPMENT ADMINISTRATION  
CONTRACT W-7405-ENG. 36

Printed in the United States of America. Available from  
National Technical Information Service  
U.S. Department of Commerce  
5285 Port Royal Road  
Springfield, VA 22161  
Price: Printed Copy \$4.00 Microfiche \$3.00

**NOTICE**

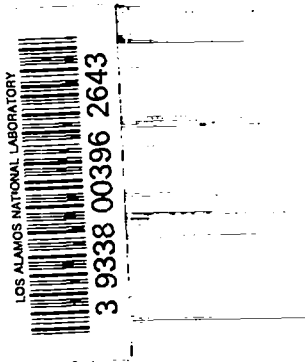
This report was prepared as an account of work sponsored by the United States Government. Neither the United States nor the United States Nuclear Regulatory Commission, nor any of their employees, nor any of their contractors, subcontractors, or their employees, makes any warranty, express or implied, or assumes any legal liability or responsibility for the accuracy, completeness or usefulness of any information, apparatus, product or process disclosed, or represents that its use would not infringe privately owned rights.

LA-NUREG-6713  
NRC-3



# Decay Heat from Products of $^{235}\text{U}$ Thermal Fission by Fast-Response Boil-Off Calorimetry

J. L. Yarnell  
P. J. Bendt



Manuscript completed: February 1977  
Issued: September 1977

# DECAY HEAT FROM PRODUCTS OF $^{235}\text{U}$ THERMAL FISSION BY FAST-RESPONSE BOIL-OFF CALORIMETRY

by

J. L. Yarnell and P. J. Bendt

## ABSTRACT

A cryogenic boil-off calorimeter was used to measure the decay heat from the products of thermal-neutron-induced fission of  $^{235}\text{U}$ . Data are presented for cooling times between 10 and  $10^5$  s following a  $2 \times 10^4$  s irradiation at constant thermal-neutron flux. The experimental uncertainty ( $1 \sigma$ ) in these measurements was  $\approx 2\%$ , except at the shortest cooling times where it rose to  $\approx 4\%$ . The beta and gamma energy from an irradiated  $^{235}\text{U}$  sample was absorbed in a thermally isolated 52-kg copper block that was held at 4 K by an internal liquid helium reservoir. The absorbed energy evaporated liquid helium from the reservoir and a hot-film anemometer flowmeter recorded the evolution rate of the boil-off gas. The decay heat was calculated from the gas-flow rate using the heat of vaporization of helium. The calorimeter had a thermal time constant of 0.85 s. The energy loss caused by gamma leakage from the absorber was  $\leq 3\%$ ; a correction was made by Monte Carlo calculations based on experimentally determined gamma spectra.

The data agree within the combined uncertainties with summation calculations using the ENDF/B-IV data base. The experimental data were combined with summation calculations to give the decay heat for infinite ( $10^{13}$  s) irradiation. For short cooling times, the results are  $\approx 7\%$  below the current American Nuclear Society (ANS) standard. The uncertainty in these results is significantly smaller than that assigned to the standard.

---

## I. INTRODUCTION

This report describes calorimetric measurements of the total decay heat from the products of thermal-neutron-induced fission of  $^{235}\text{U}$ . Data are presented for cooling times between 10 and  $10^5$  s following a  $2 \times 10^4$  s irradiation at constant thermal-neutron flux. The experimental uncertainty ( $1 \sigma$ ) in these measurements was  $\approx 2\%$ , except at the shortest cooling times where it rose to  $\approx 4\%$ .

This work was carried out at the Los Alamos Scientific Laboratory (LASL) as part of a program sponsored by the U.S. Nuclear Regulatory Commission (NRC) to provide better values and reduced uncertainties for the decay heat source term for use in reactor safety evaluations and, in particular, for analysis of the Loss-of-Coolant Accident (LOCA).

There have been many measurements of decay heat. Unfortunately, there is considerable scatter in

the results of individual experiments. (See, for example, the review by Perry, Maienschein, and Vondy.<sup>1</sup>) The present American Nuclear Society (ANS) Decay Heat Standard<sup>2</sup> reflects the state of knowledge when it was prepared by specifying an uncertainty band of +20%, -40% for cooling times < 10<sup>3</sup> s, which are important in LOCA analysis.

Calorimetric measurements have the advantage that they are relatively simple and straightforward, require only minor corrections, and thus present a minimum opportunity for the introduction of systematic errors. Their disadvantages are that they provide only integral information (total decay heat, not beta and gamma spectra) and that, in general, they tend to have long time constants.

Lott et al.<sup>3</sup> have reported decay heat measurements made with a conduction calorimeter. The thermal time constant of their apparatus was  $\approx 115$  s, and they estimate the uncertainty in their results to be  $\approx 5\%$ . The shortest cooling time for which they could measure decay heat was 70 s. When our experiments were undertaken, the results of Lott et al. were the best calorimetric measurements available for times pertinent to LOCA analysis.

Our measurements were carried out using a cryogenic boil-off calorimeter. In this technique, the decay heat evaporates a cryogen (in our case liquid helium) and the evolution rate of the boil-off gas is measured with a flowmeter. Since the heat of vaporization of helium is known, the amount of decay heat can be calculated from the boil-off rate, or the system can be calibrated by joule heating.

The idea of cryogenic boil-off calorimetry is not new. It was first proposed by Sir James Dewar in 1894.<sup>4</sup> In 1904, Madame Curie reported its use to measure the decay heat of radium.<sup>5</sup> We chose this method because it gave us an opportunity to develop a massive calorimeter with a short time constant.

This development involved the construction and testing of a prototype calorimeter, as well as numerous auxiliary measurements and calculations. A final model of the calorimeter was designed on the basis of information thus obtained.<sup>6</sup> It was tested extensively to determine its characteristics and to optimize experimental procedures. It had a thermal constant of < 1 s, even though it contained a radiation absorber that weighed 52 kg. The short response time was achieved by operating the calorimeter

nearly isothermally, and by taking advantage of the large decrease in the heat capacity of solids that occurs when the temperature is lowered to the boiling point of helium (4 K).

A preliminary report of our decay heat measurements was presented at the Fourth Water Reactor Safety Information Meeting in September 1976.<sup>7</sup>

## II. EXPERIMENTAL DETAILS

### A. Samples: Preparation, Irradiation, and Transfer

In these measurements, samples of <sup>238</sup>U were irradiated in a constant thermal-neutron flux of  $\approx 3 \times 10^{18}$  n/cm<sup>2</sup>·s. The irradiation time of  $2 \times 10^4$  s was chosen to be long compared to the times of greatest interest in LOCA analysis, yet short enough to be compatible with the single-shift operation of the Los Alamos Omega West Reactor (OWR). The OWR is an 8-MW, tank-type research reactor that uses 93%-enriched uranium fuel with light water coolant and moderator.

To obtain decay heat data at short cooling times, the samples must be transferred to the calorimeter and cooled to the temperature of liquid helium as rapidly as possible. In addition, they must produce decay heating rates commensurate with the dynamic range of the calorimeter ( $\approx 3400$  to 70 mW) and must be provided with a cladding to prevent the loss of gaseous fission products during irradiation and transfer. (During the measurements, the samples were at 4 K and all fission products were solids.) Using the samples and transfer system described below, the samples reached the calorimeter  $\approx 1.5$  s after irradiation; cooldown was essentially complete 3 s later.

The samples contained 33-mm-long by 5-mm-wide by 0.02-mm-thick uranium foils that weighed  $\approx 60$  mg. The isotopic composition of each foil was 0.87 wt% <sup>234</sup>U, 93.19 wt% <sup>235</sup>U, 0.48 wt% <sup>236</sup>U, and 5.46 wt% <sup>238</sup>U. The foils were placed in envelopes of 0.127-mm-thick aluminum, which were then sealed by electron-beam welding. The completed samples were 39 mm long by 8 mm wide by 0.3 mm thick. They weighed  $\approx 300$  mg. Aluminum was chosen for the envelopes because of its minimum interference

with the radiochemical procedures used to determine the number of fissions in the sample. To provide good heat transfer between the uranium and aluminum, the uranium was electropolished before being inserted in the envelopes, and the envelopes were carefully flattened after sealing. The low mass and large surface area of the samples promoted rapid cooldown when the samples were dropped into the liquid helium in the calorimeter.


The envelopes were checked for external uranium contamination by alpha counting. They were leak-tested before use by immersing them in liquid helium for 30 min, followed by rapid warming to room temperature. Samples that were tight remained flat, whereas those that leaked swelled because of the rapid expansion of the helium that penetrated the weld. We opened the defective samples and placed the uranium foils in new envelopes.

A dart was used to transport the samples from the irradiation position near the core of the OWR to the sample release chamber above the calorimeter (see Fig. 1). At the start of irradiation, the dart (with encased sample) was pushed into position with a long, flexible plastic rod. At the end of the irradiation, the dart was ejected by pressurized helium gas. It took only a fraction of a second for the dart to reach and stick in a wooden target in the sample release chamber (a distance of  $\approx 5$  m).

The dart was made of two pieces of aluminum, hinged at the forward end and tapered slightly toward the rear. The sample was placed between the two pieces of the dart, which were held together by an outer steel sleeve. The sleeve was stripped off as the dart entered the sample release chamber. When it struck the wooden target, the dart opened, releasing the sample. The sample then fell into a funnel where it was guided into a tube that led to the liquid helium reservoir in the calorimeter.

The irradiation position in the OWR is shown in Fig. 2. During an irradiation, the reactor power was controlled by a fission chamber adjacent to the sample. The neutron flux at the sample position, when averaged over 10-s intervals, was constant to within  $\pm 0.1\%$  during the irradiation.

Water was circulated through a spiral channel in the aluminum cylinder (shown in Fig. 2) to remove the 70 W of fission heat that developed in the uranium foil as well as the gamma heat from the reactor environment. Helium gas circulated around


  
 Sample
   
 39 mm x 8 mm x 0.3 mm
   
 ~ 60 mg 93%  $^{235}\text{U}$ 
  
 ~ 240 mg Al clad

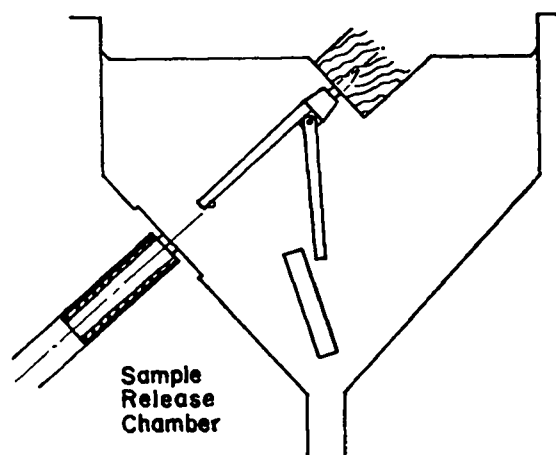
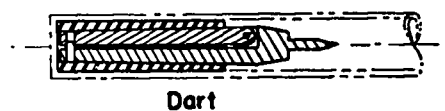


Fig. 1.

*Sample, transport system (dart), and sample release chamber used for decay heat measurements. During irradiation, the sample is encased in the dart. At the end of the irradiation, the dart is blown into the release chamber, where the outer sleeve of the dart is stripped away, and the sample is freed to fall into the calorimeter.*

the dart and transferred heat to the water-cooled cylinder. The exhaust helium gas passed through an activated charcoal filter adjacent to a NaI(Tl) radiation detector, which was a sensitive and rapid monitor of any radioactivity (fission-product gases) that escaped from the sample. Any leakage from a sample was discovered within a few seconds after the start of irradiation, and the sample was ejected immediately into a standby shielded "pig." All the tubes leading into the reactor port were spiraled around graphite and brass forms to reduce radiation leakage from the port during the irradiation.

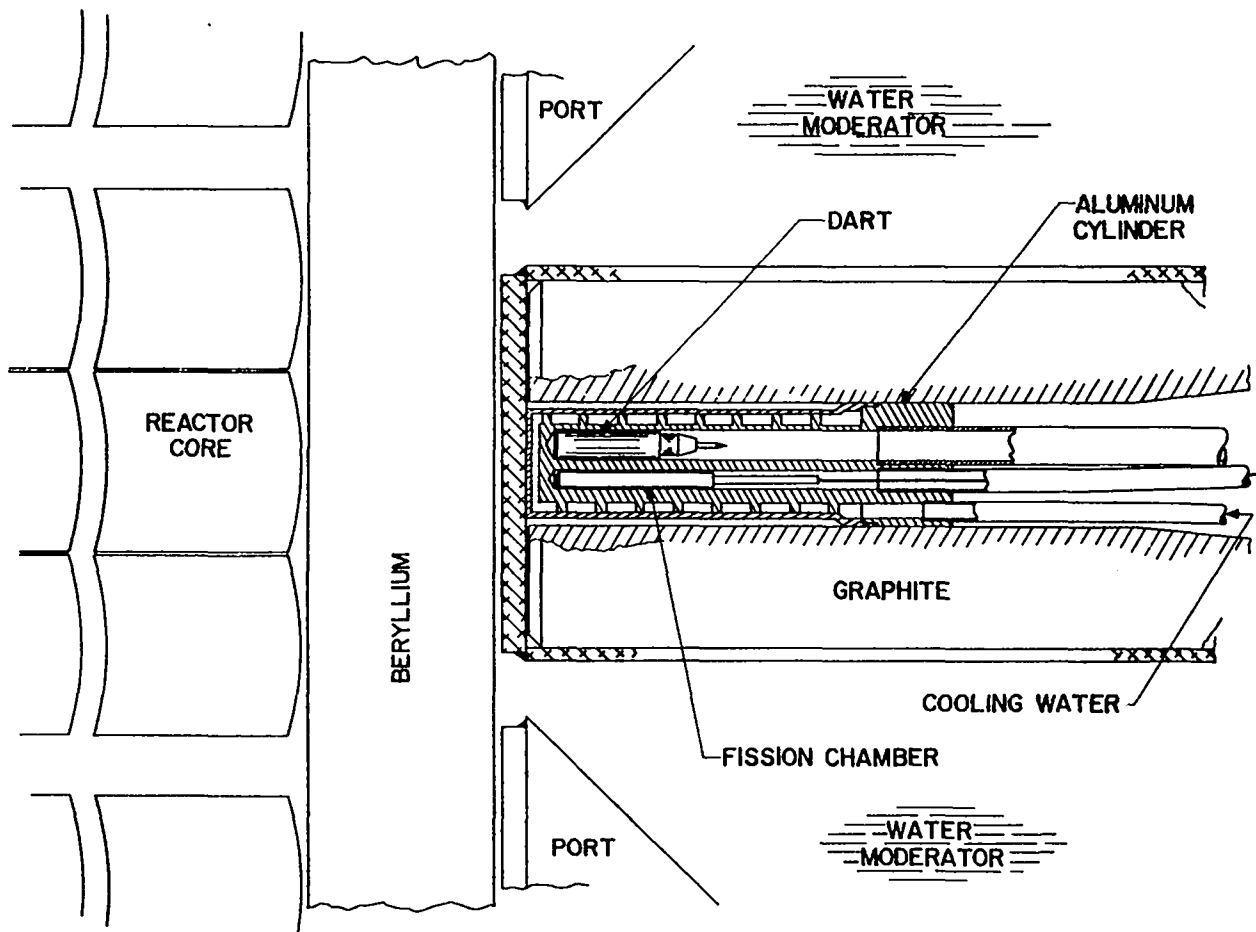


Fig. 2.

Facility used for sample irradiation. The facility is located in one of the 152-mm-diam ports of the 8-MW OWR. The port walls are made of aluminum. The fission chamber adjacent to the sample was used to control the reactor power during irradiation.

In the neutron spectrum at the irradiation position, the fission rate per unit mass was determined experimentally to be  $\approx 10^4$  times smaller for  $^{238}\text{U}$  than it was for  $^{235}\text{U}$ . Since the samples contained  $\approx 6\%$   $^{238}\text{U}$ , the fraction of the fissions that occurred in  $^{238}\text{U}$  was  $\approx 0.0006\%$ . We calculate that under the experimental conditions, contributions to the measured decay heat from neutron capture in fission products and from production of  $^{239}\text{U}$  and  $^{239}\text{Np}$  also were negligible.

### B. Calorimeter and Auxiliary Apparatus

The main features of the calorimeter are shown in Fig. 3. The copper block, which absorbed  $\geq 97\%$  of

the radiation energy emitted by the sample, was 177.8 mm in diameter, 298.5 mm high, and weighed 52.008 kg. The reservoir in the top of the block was filled with 1.2 liters of liquid helium. The block was suspended in vacuum by means of a 10-mm-i.d. thin-wall stainless steel tube that was used to transport the boil-off gas to a flowmeter at room temperature. The tube was also used to insert and remove the samples and to transfer the liquid helium to the reservoir.

To provide a source of electric heating for calibration and testing, a 196- $\Omega$  coil of Manganin wire was wound in a groove 10 mm from the bottom of the block. The groove was then filled with Stycast

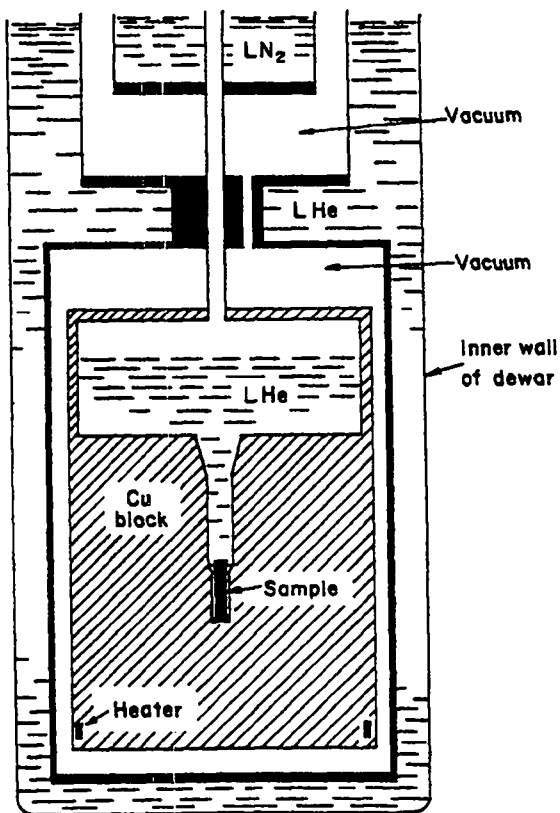


Fig. 3.

Active portion of the boil-off calorimeter. Radiation from the sample was absorbed in the copper block and was used to evaporate liquid helium from the reservoir in the top of the block. Heat leak into the copper block was prevented by the vacuum jacket and the outer helium bath.

2850FT epoxy\* to ensure good thermal contact between the wire and the block. A copper band was pressed over the block in the groove area so that the coil was completely surrounded by copper. This was done to ensure that all of the energy produced in the coil was transferred to the block and none was radiated directly to the surroundings.

Not shown in Fig. 3 are a liquid helium level sensor and a germanium resistance thermometer (GeRT) in the reservoir, and three GeRTs attached to the block. The GeRTs could detect temperature changes of 1 mK and had an absolute accuracy of  $\approx 5$  mK.

\*Manufactured by Emerson and Cuming, Inc., Canton, MA 02021.

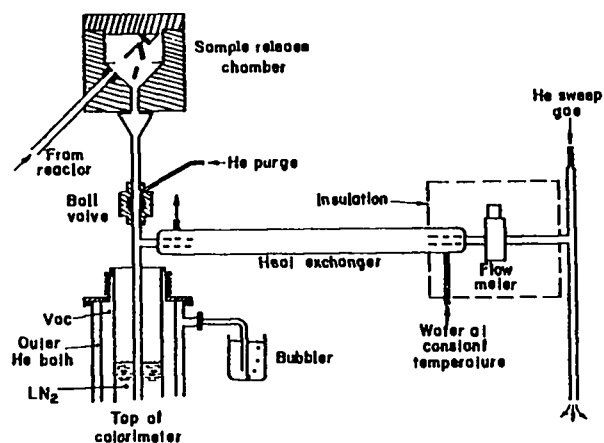


Fig. 4.

Upper portion of the boil-off calorimeter showing the piping used to transport the boil-off gas to the flowmeter. The ball valve was opened briefly to permit entry of the sample. The helium purge gas and sweep gas prevent air from entering the boil-off gas stream.

To prevent heat leak, a copper vacuum jacket immersed in an outer liquid helium bath surrounded the calorimeter block. A commercial liquid-nitrogen-jacketed dewar contained the entire assembly. A level sensor was provided for the outer helium bath. All electrical leads reaching the calorimeter block passed through the outer helium bath, which intercepted heat conducted along the leads from warmer regions.

The calorimeter was assembled by high-temperature brazing in a hydrogen furnace. The upper portion of the calorimeter system is shown in Fig. 4. The irradiated samples fell from the sample release chamber into the calorimeter through a remotely operated ball valve. When the ball valve was closed, the boil-off gas passed through a fast-response flowmeter and was discharged to the atmosphere. To keep air from entering the system, helium purge gas was injected above the ball valve before and during the time it was open, and a constant small flow of helium sweep gas was injected downstream of the flowmeter. (Air contamination of the boil-off gas would cause incorrect flowmeter readings.)

The outer helium bath was kept at 15 torr above atmospheric pressure by venting it through a bubbler. This raised its temperature 25 mK above the



boiling point of the liquid helium in the reservoir (which was within 1 torr of atmospheric pressure) and prevented the boil-off gas from condensing on the tube walls after it left the reservoir.

The helium that was evaporated was warmed to room temperature in a controlled manner. Although the flowmeter was temperature compensated, we found the accuracy of the flow measurements could be improved if the boil-off gas from the calorimeter was warmed to the temperature at which the flowmeter had been calibrated. The significant precaution about warming the helium gas from the calorimeter was to minimize changes in the temperature distribution along the gas transport tube, since such changes varied the gas storage in the tube and thereby distorted the time profile of the gas flow rate. This precaution was especially important at low temperatures where the gas density was high. We have dealt with this problem by having long sections of tubing at fixed temperatures and by minimizing the volume of the lengths of tubing between fixed temperatures.

After leaving the copper block, the boil-off vapor first flowed through tubing that had good thermal contact with the outer helium reservoir (Fig. 3). The vapor next passed through a short length of thin-wall tubing in vacuum, then through a long tube in thermal contact with a liquid nitrogen bath, which raised the helium temperature above the critical point. The liquid nitrogen was stirred by convection generated by a 20-W heater, which also replaced heat removed by the flowing helium gas, so that nitrogen was not solidified on the outside surface of the gas transport tube. When the helium gas reached the top of the cryostat, it flowed through a horizontal heat exchanger (see Fig. 4). Water flowed at 4.5 liters/min at a constant 27°C through the outer jacket of the heat exchanger. The gas entering the flowmeter was at a constant 26.5°C. When the flowmeter was calibrated with helium from a pressurized tank, using a pressure reducer and needle valve, the bottled gas also flowed through the heat exchanger and emerged at the same temperature. The gas temperature was measured by a thermocouple in the flow line, just beyond the flowmeter, and was displayed on a chart recorder.

The flowmeter was of the hot-film anemometer type\* (Fig. 5). It was sensitive to mass flow and had

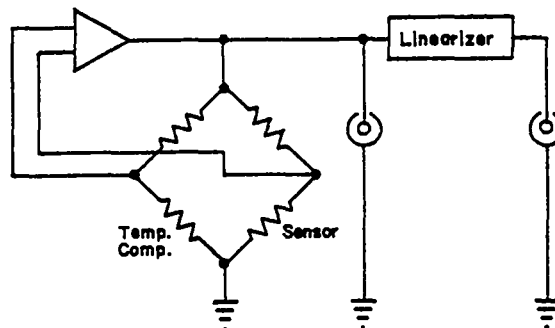
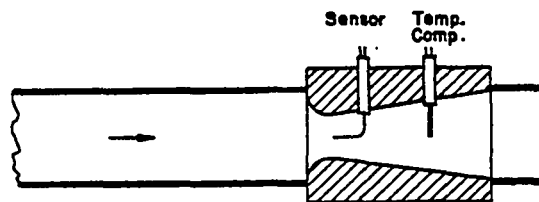


Fig. 5.

*Details of the hot-film anemometer-type flowmeter. The feedback circuit maintains the hot-film sensor a constant number of degrees above the temperature of the gas stream. The voltage required across the bridge to accomplish this is a measure of the mass flow through the flowmeter.*

a time constant of  $\approx 1$  ms. A smooth venturi placed in the gas-flow stream was designed so that the flow velocity was uniform over the cross section of the throat. A sensor, consisting of a platinum film resistor on a quartz fiber, was located in the venturi throat. Heat was supplied to the film electrically and removed by the flowing gas. A temperature-compensating resistor was placed downstream of the sensor. The sensor and compensating resistor formed two arms of a bridge; a feedback circuit varied the voltage across the bridge to keep the difference between the film temperature and the gas temperature constant (at  $\approx 225^\circ\text{C}$ ). Under these conditions, the bridge voltage is represented approximately by the equation

$$V^2 = A + B(T_s - T_g)(\rho v)^{1/n} \quad ,$$

\*Manufactured by Thermo-Systems, Inc., St. Paul, MN 55113.

where A and B are constants,  $T_s$  and  $T_g$  are the sensor and gas stream temperatures, respectively,  $\rho$  is the gas density and  $v$  is its velocity, and  $1/n$  is an exponent approximately equal to  $1/2$ . The constants depend on the composition of the gas and on the construction of the flowmeter. This equation illustrates the nonlinear relation between the flowmeter output,  $V$ , and the mass flow,  $\rho v$ .

In our decay heat measurements, the bridge voltage, the primary quantity recorded, was converted to heating rate by means of an experimentally determined calibration curve rather than by the above equation. By using an electronic linearizing circuit, the flowmeter also generates a signal approximately linear in  $(\rho v)$ . This signal was used to monitor the progress of the measurements. However, we did not use the linearizer output to calculate any of the final results. The flowmeter was custom designed to produce the minimum pressure drop consistent with the required sensitivity. To stabilize its temperature, the flowmeter was enclosed in Styrofoam.

The instrumentation used to monitor the calorimeter and record the flowmeter measurements is shown as a block diagram in Fig. 6. The bridge voltage from the mass flowmeter was converted to a pulse train of variable frequency by a voltage-to-frequency (V/F) converter,\* then counted by a 4096-channel Geoscience Digital Processor\*\* operated in the multiscaler mode. In this mode, counts are accumulated for a predetermined time in successive memory channels. During the first 4095 s of cooling time, we used 1-s-wide channels; at longer times we used 10-s-wide channels. The digital processor had a quartz-crystal-controlled clock that provided the time base for the measurements. The data were read out onto magnetic tape and processed in a digital computer. Tests at the LASL electrical standards laboratory showed that the linearity of the V/F converter was better than 0.02%. Its slewing rate of  $10^6$  V/s was more than sufficient to follow the 1-ms response of the flowmeter.

The flowmeter output was recorded by three other instruments, in addition to the digital processor. The linear output was recorded on two strip chart recorders, whose gains differed by a factor of 2, to extend the dynamic range. The bridge voltage, after

being converted to a pulse train by a V/F converter, was counted by a frequency counter and printed on paper tape. Also printed on the paper tape was the temperature (in millikelvin) of the copper block in the calorimeter. The counting intervals for the frequency counter were determined precisely by an internal quartz-crystal-controlled clock. Although the printer introduced a dead time of  $\approx 0.1$  s between counts, it caused no errors since the paper tape output was not used for precise timing measurements.

The voltage and current supplied to the electric heater in the copper block during calibration measurements were also converted to a pulse train by a second V/F converter and printed on paper tape. The current was recorded by measuring the voltage drop across an external 10.004- $\Omega$  standard resistance. A transfer standard\* provided 1.0000 reference volts for calibrating the V/F converters. The temperature of the helium gas passing through the flowmeter was recorded continuously on a strip chart recorder. The liquid helium level sensors and GeRTs, shown in Fig. 6, were used in operating the liquid helium calorimeter. Several vacuum gauges, thermometers, gas flowmeters, and a helium leak detector were also used.

A timing sequencer controlled the transfer of the sample from the irradiation position to the calorimeter in a reproducible manner. Let  $t = t_0$  be the time that the signal to eject the dart was initiated, at the end of a  $2 \times 10^4$  s irradiation. At  $t_0 - 20$  s, the flow of helium purge gas above the ball valve was started and at  $t_0 - 5$  s, the ball valve was opened. At  $t_0 - 0.5$  s, the multiscaler was started (using 1-s time channels) so that the center of channel 0 occurred at  $t_0$ , the center of channel 1 occurred at  $t_0 + 1$  s, and so on. At  $t_0 + 4$  s, the ball valve was closed. These times were chosen, after trying various combinations, because they minimized the disturbance to the system that followed transfer of the sample. The flow of helium purge gas was set to a value that had been shown previously to prevent air from entering the system through the ball valve.

The fission chamber adjacent to the irradiation position provided a convenient means of checking the timing. When the dart was being irradiated, it depressed the flux at the fission chamber by  $\approx 4\%$ . The 4% rise in fission chamber signal when the dart

\*Manufactured by Hewlett Packard Co., Palo Alto, CA 94303.

\*\*Manufactured by Geoscience Nuclear, Hamden, CT 06518.

\*Manufactured by John Fluke Manufacturing Co., Mountlake Terrace, WA 98043.

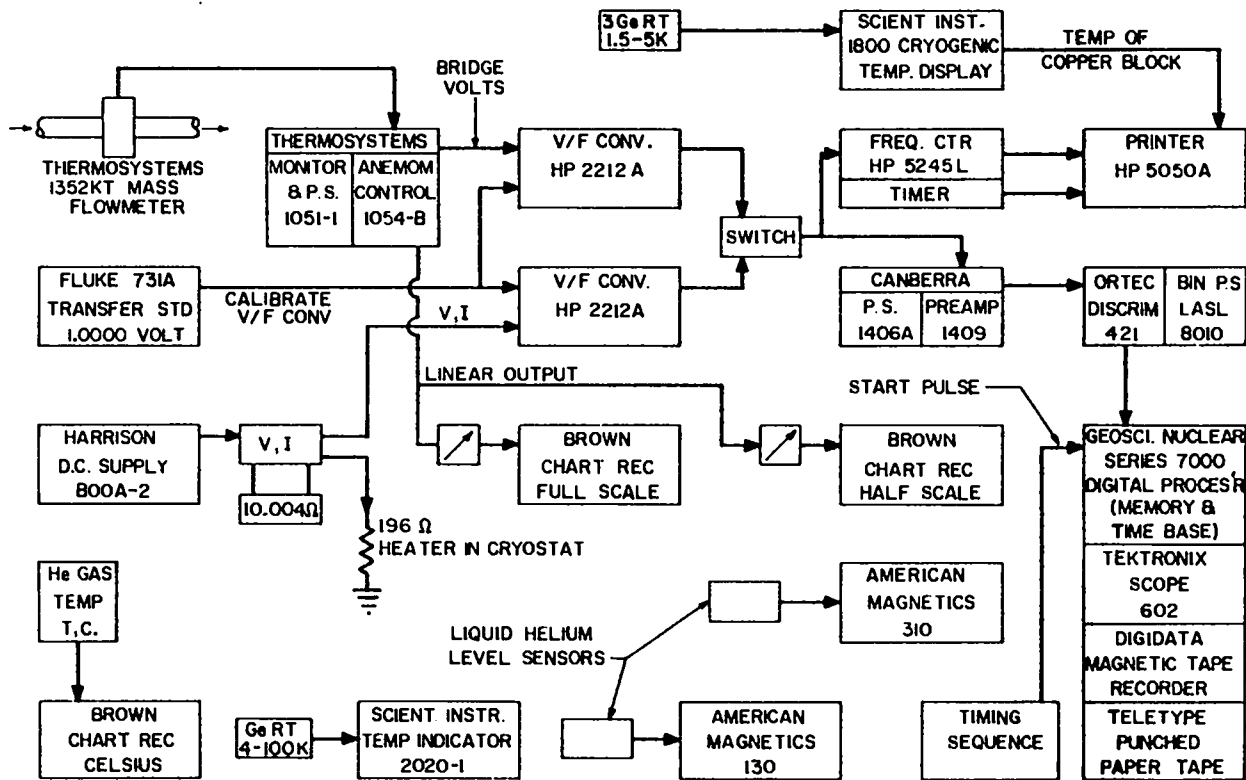


Fig. 6.

Block diagram of instrumentation used to monitor the boil-off calorimeter and record decay heat data.

left the irradiation position provided an accurate indication of the end of the irradiation. The time interval between the start of the multiscaler and the end of the irradiation was found to be  $0.65 \pm 0.02$  s; consequently, the center of the  $n$ 'th 1-s time channel corresponded to a cooling time of  $(n - 0.15)$  s. This correction was applied when analyzing the data.

### C. Performance of the Calorimeter

The calorimetric measurement was made as nearly isothermally as possible, in order that nearly all the radiation energy deposited in the copper absorber would evaporate liquid helium instead of being stored in the form of thermal energy. Such energy storage lengthens the response time of the calorimeter.

Since we had a two-phase system, the temperature of the liquid helium was dependent on the

pressure in the reservoir, and could be determined from the saturated vapor-pressure curve.<sup>8</sup> With maximum helium gas flow, the pressure drop along the transport tube and across the flowmeter is  $\leq 1$  torr, and, therefore, the liquid helium temperature does not rise during the measurements by more than 1.7 mK. [At one Los Alamos atmosphere ( $\approx 598$  torr), the liquid temperature is  $\approx 3.967$  K.] The heat capacity of the 1.2 liters of liquid helium in the reservoir at the start of a measurement was  $\approx 550$  J/K, so the maximum energy storage in the liquid helium was  $\approx 1$  J.

The heat capacity of the 52-kg copper block at 4 K was only 4.4 J/K, and since the maximum temperature rise of the block (measured with a GeRT) during a decay heat measurement was 40 mK, energy storage in the block was only 0.2 J.

The copper block which was made of well-annealed oxygen-free high-conductivity copper had a high thermal conductivity at 4 K. Measurements

with GeRTs located at the top and bottom of the block indicated a temperature difference of  $\leq 1$  mK when 3000 mW was supplied by the heater coil and removed by the evaporation of liquid helium. The large thermal conductivity and low heat capacity at 4 K resulted in a thermal diffusivity of  $\geq 3000$  cm<sup>2</sup>/s and a thermal time constant of  $\leq 0.16$  s. (For comparison, the diffusivity at room temperature of the copper block is  $\approx 1.1$  cm<sup>2</sup>/s, and the time constant is  $> 400$  s.) We conclude that the temperature of the copper block was uniform (within 1 mK) at all times.

The reservoir was made broad and shallow to increase the copper-liquid surface area and to reduce the maximum liquid depth above the shelf in the reservoir (56 mm). The 40 mK temperature rise of the copper block is the  $\Delta T$  necessary to transfer  $\approx 3$  W across the copper-liquid interface. Convection currents in the liquid helium, initiated by thermal cooling of the irradiated sample, provided rapid heat transport to the liquid-vapor interface. We observed superheating of the liquid helium only when it was quiescent. Dropping a thermally hot ( $\approx 380$  K) irradiated sample into the calorimeter always provided sufficient disturbance to eliminate superheating.

When it first evaporated, the helium vapor was at the same temperature as the liquid; the reservoir walls however were slightly warmer. Because a small amount of heat flowed directly into the vapor instead of into the liquid, it was not recorded by the flowmeter measurement. The maximum possible error was  $(C_p \Delta T)/L$ , where  $C_p$  was the heat capacity of the vapor,  $\Delta T$  was the temperature rise of the copper block, and  $L$  was the latent heat of evaporation. During decay heat measurements, when the  $\Delta T$  was at its maximum value of 40 mK, the maximum possible correction was 1.6%. However, the actual correction was much smaller because of inefficient heat transfer to the vapor. After calculating the heat transfer by two approximate methods, we concluded that the correction was  $\leq 0.3\%$ . This was confirmed by the good agreement between calibration curves, determined from accurate knowledge of gas flow and latent heat (which were subject to the correction), and calibrations based on electric heating (which automatically included the correction).

The heat leak into the copper block was caused mainly by conduction along the thin-wall stainless

steel tube and the electrical leads that connect the block to the vacuum jacket (which was at the temperature of the outer helium bath). The heat leak was therefore proportional to the temperature difference between the block and the outer helium bath and was determined experimentally to be 800  $\mu$ W/K. During decay heat measurements, the heat leak varied from  $+20$   $\mu$ W when the copper block was at the temperature of the liquid helium in the reservoir to  $-12$   $\mu$ W when the copper block was 40 mK warmer than the helium. This heat leak was so small that it was neglected.

The time constant of the calorimeter was measured by making step changes in electric power to the heater in the copper block while recording the flowmeter output. For changes between power levels that were both  $> 70$  mW, the response was well represented by the expression

$$P(t) = P_1 + (P_r - P_1)(1 - e^{-t/R})$$

where  $P(t)$  is the indicated response  $t$  seconds after a step change in input power from  $P_1$  to  $P_r$  and  $R$  is the exponential time constant. Ten measurements that included both increases and decreases in input power yielded a value of  $0.85 \pm 0.09$  s for  $R$ . Figure 7 shows typical response curves for step decreases in electric power input.

When the input power dropped to zero, the flowmeter response no longer followed a single exponential decay. Below  $\approx 70$  mW the apparent time constant increased as the power decreased, producing a long tail on the response curve. The decay heat was changing very slowly by the time ( $\approx 3 \times 10^4$  s) it had fallen to 70 mW, so the increased response time in this power range was not a problem.

Since the thermal time constant of the copper block was estimated to be  $\leq 0.16$  s, it was clear that the calorimeter's response was dominated by the time constant of the helium transport and measurement system. We verified this by supplying constant electric power input to the heater, and then opening and closing the ball valve. The recovery shown by the flowmeter when the ball valve was closed was similar to its response to a step increase in power, indicating that an important contribution to the response was the time required to build up pressure across the flowmeter. For this reason it was important to select a flowmeter that had a small

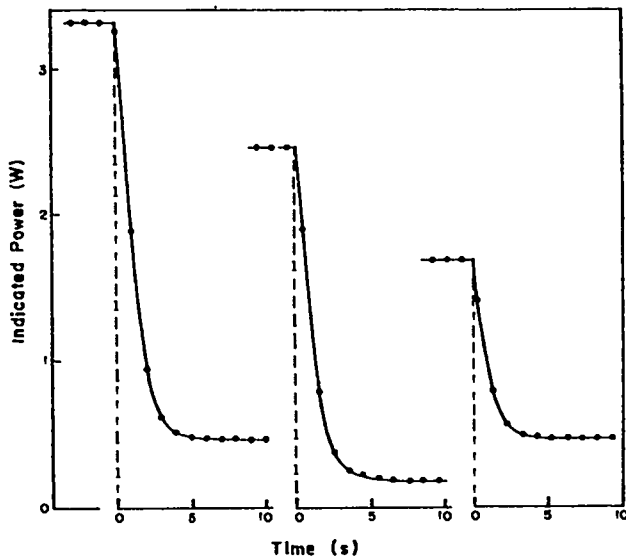


Fig. 7.

Calorimeter response to step decreases in electric heater power input. The curves are typical of the response to both increases and decreases in power (when the minimum power is  $\approx 70$  mW). The curves are well represented by a single exponential with a time constant of  $0.85 \pm 0.09$  s. For power decreases to  $< 70$  mW, the response curve shows a long tail in addition to the initial exponential decay.

pressure drop at the desired flow rates. (A second reason was to minimize the changes in the boiling point of the helium in the inner reservoir.)

Since the process of boiling is subject to fluctuations, the output signal from the flowmeter contained a noise component. The RMS noise, evaluated for a 1-s averaging time, varied from  $\approx 0.65\%$  at 100 mW to  $\approx 0.25\%$  at 3000 mW. Our method of recording data automatically provides averaging over 1- or 10-s intervals. Additional smoothing was provided in the data analysis.

The charge of liquid helium in the reservoir was exhausted after 4000 to 6000 s, depending on the initial filling. At this point the reservoir was refilled and the multiscaler was restarted at a known clock time, using 10-s time channels. For measurements out to a cooling time of  $10^6$  s, a second refill was required. The reservoir was refilled at different times for different runs to attain continuous coverage.

#### D. Calibration of the Flowmeter

Because the relation between the flowmeter bridge voltage and the mass flow of helium gas is given only approximately by theory, a calibration curve had to be established experimentally. This was done by running two independent series of measurements. In the first series, known rates of electric heating were supplied to the coil in the copper block. This had the advantage of checking the entire helium boil-off and gas-transport system. In the second series, the mass flowmeter was checked with steady-state flows of helium gas against the integrated volumes measured with a diaphragm-type test meter\* that had been calibrated by the manufacturer using a one-cubic-foot bottle certified by the US National Bureau of Standards. Both tests were repeated each day a uranium sample was irradiated to determine whether the calibration changed between runs. There was no evidence of changes in calibration, so the same calibration curve was used to convert all flowmeter bridge voltages, digitally recorded during decay heat measurements, into milliwatts deposited in the radiation absorber.

Electric calibration measurements were taken by determining both the voltage,  $V$ , and current,  $I$ , supplied to the electric heater. Currents were determined by measuring the voltage drop across an external  $10.004\text{-}\Omega$  standard resistance. Voltages were measured by comparing them to a 1-V Fluke Transfer Standard, which was calibrated against an Epply Standard Cell from the Primary Standards Laboratory of the Sandia Laboratories. Voltages were accurate to  $\pm 0.002\%$ ; currents and electric power were accurate to  $\pm 0.01\%$ .

The resistance of the calorimeter heater plus leads varied from  $194.5\ \Omega$  at 30 mW to  $196.0\ \Omega$  at 3 W (at 4 K). The resistance of the copper lead wires was  $\approx 0.8\ \Omega$ , nearly all of which occurs along parts of the wires in the helium vapor above the liquid level in the outer helium reservoir. Using an average value for the heater resistance, we found that 0.996 of the electric heat was deposited in the calorimeter; we therefore used the expression

\*Such meters are often called dry test meters to distinguish them from liquid-sealed rotating-drum meters, which are known as wet test meters. For further discussion see the American Society for Testing and Materials Standard D 1071.

$$mW = 996 (V \cdot I).$$

The gas flow calibration points were measured with an American Meter Company Model DTM-115 dry test meter.\* The manufacturer's calibration curve showed variations from the nominal reading to be  $\leq 0.2\%$  over the range of flow rates we used. During calibration measurements, helium gas entered the gas transport system just ahead of the heat exchanger (see Fig. 4), and the dry test meter was connected to the exhaust side of the anemometer flowmeter. Liters per second of steady-state gas flow, measured at atmospheric pressure and room temperature with the dry test meter and a stop watch, were converted to flow rates at 760 torr and  $0^\circ\text{C}$  using the ideal gas law. Under these conditions, 1 mole occupied 22.4136 liters.<sup>9</sup>

Since about 10% of the vapor evaporated from liquid helium did not reach the flowmeter, but remained in the reservoir in the volume formerly occupied by liquid, it was necessary to know the "apparent" heat of vaporization,  $L_a$ , in order to convert the observed gas flow to watts.  $L_a$  is related to the true heat of vaporization,  $L$ , by

$$L = L_a(1 - V_L/V_G) \text{ J/mole,}$$

where  $V_L$  and  $V_G$  are the molar volumes of liquid and gas, respectively. The most precise measurement of  $L_a$  has been made by Ter Harmsel, van Dijk, and Durieux,<sup>10</sup> who also reviewed and compared earlier measurements.<sup>11,12</sup> Their smoothed data gives a value of  $L_a = 97.91 \text{ J/mole}$  ( $\pm 0.13\%$ ) at  $3.967 \text{ K}$ , which corresponds to a saturated vapor pressure of 598.3 torr, using the 1958-<sup>4</sup>He temperature scale. Using these numbers, it can be determined that a gas flow rate of 1 liter/s at Los Alamos atmospheric pressure corresponds to  $\approx 3.15 \text{ W}$ . (The exact value depends on the temperature and pressure of the gas in the dry test meter.)

The final calibration curve was a least squares fit of a 10-point cubic spline to 94 gas-flow calibration points and 70 electric-heating calibration points. The uncertainty in the calibration curve was estimated from the accuracy of the standards ( $\approx 0.2\%$ ) and from an analysis of the deviations of the individual calibration points from the fitted curve. The total uncertainty ( $1 \sigma$ ) assigned to the

\*Manufactured by Singer, American Meter Division, Philadelphia, PA 19116.

fitted calibration curve varied from 0.5% for powers  $> 800 \text{ mW}$  to 2.2% at  $70 \text{ mW}$ . For powers  $> 400 \text{ mW}$  (where the calibration is the most accurate), the algebraic sum of the percent deviations of the electric-heating calibration points from the fitted curve was  $+0.02\%$ . The corresponding value for the gas-flow calibration points was  $-0.01\%$ . We conclude that there was no significant difference between the two calibration methods.

We took  $70 \text{ mW}$  to be the lower limit of the useful range of the anemometer flowmeter for accurate decay heat measurements. For power levels  $< 70 \text{ mW}$ , where the decay heat was changing slowly (cooling times were  $> 3 \times 10^4 \text{ s}$ ), we made integral flow measurements with the dry test meter described above. We estimate a 1% uncertainty in these measurements, based on discussions with the manufacturer of the flowmeter concerning the accuracy to be expected at these (low) flow rates.

### III. FISSION RATES

The calorimetric measurements yield the energy release rate, in  $\text{MeV/s}$ , as a function of cooling time. This rate must be divided by the fission rate in the sample during irradiation to obtain the normalized decay heat in  $\text{MeV/s}$  per fission/s (often abbreviated  $\text{MeV/fiss}$ ).

Since the flux at the sample position was held constant (to  $\approx 0.1\%$ ) during the irradiation, the average fission rate was obtained by dividing the total number of fissions in the sample by the irradiation time. The determination of total fissions was carried out by the LASL Radiochemistry Group (CNC-11), which has had many years experience in connection with fission yield measurements for the LASL Weapons Test Program.

#### A. Sample Dissolution

After a calorimetric measurement had been completed and the calorimeter had returned to room temperature, the sample was removed from the copper block with a special handling tool and placed in a shielded container. It was later transferred to a hot cell, where it was dissolved in  $3 \text{ M HCl}$ , to which a small amount of  $\text{HNO}_3$  was added to ensure dissolution of the uranium. The total volume was made up

to 1 liter in a volumetric flask, using additional 3 M HCl. Specimens containing a known fraction of the original 1-liter solution were prepared by pipetting and dilution for use in subsequent analyses.

## B. Radiochemistry and Beta Counting

In one analytical method, a standardized radiochemical (RC) procedure<sup>13</sup> was used to separate the activity due to a specific fission product, which was then counted in a standard beta proportional counter. The ratio between the counting rate of this counter (corrected for decay) and the number of fissions in the specimen is known as the K-factor for that particular activity, counter, and procedure. The K-factors for several fission products have been evaluated in previous experiments, as described below.

Using this method, four determinations of <sup>99</sup>Mo and two of <sup>140</sup>Ba were carried out for each sample. The precision of the determinations, estimated from the scatter in the results for identical specimens, was consistent with previous estimates of precision based on comparison of measurements made on duplicate specimens.

## C. Gamma Counting

In a second analytical method, the gamma spectrum of an unseparated specimen was measured with a Ge(Li) detector. Six spectra were recorded from a specimen from each of the decay heat samples. The Ge(Li) detector was calibrated using liquid multigamma standards furnished by the National Bureau of Standards. The geometry used in the calibration was identical to that used in the measurements. (The same volume of solution, in the same kind of container, at the same distance from the counter, was used.)

The gamma spectra from the specimens were analyzed using a version\* of the computer program GAMANAL,<sup>14</sup> which contains a library\*\* of spectra for individual fission products. The program performs a least squares fit of all the gamma rays from each selected nuclide and returns the number of

\*Modified for use on the LASL computers by Bruce Erdal.

\*\*The gamma ray library was compiled from literature sources by P. Grant, G. Butler, and B. Erdal.

atoms of that nuclide (corrected for decay) present in the specimen. The fitting program also estimates the statistical precision of each determination. The final results are weighted averages from the six spectra. The activities <sup>90</sup>Zr, <sup>99</sup>Mo, <sup>140</sup>Ba-La, <sup>141</sup>Ce, and <sup>147</sup>Nd were determined using the Ge(Li) counting method.

Previous calibrations had established the relation between the indicated number of atoms of a particular fission product and the number of fissions in the sample. In these calibrations, the number of fissions was obtained by RC determinations of <sup>99</sup>Mo, which are considered to be the most accurate (smallest systematic error).

The final number of fissions for each sample was taken to be the weighted average of the individual determinations. The precision of the weighted averages was estimated to be  $\approx 0.3\%$ , where the indicated precision is the larger of (1) the value obtained from the estimates of precision for the individual determinations or (2) the value obtained from the scatter of the results of the individual determinations. Results of the determinations and the estimated precisions ( $1\sigma$ ) for the three samples used in our decay heat measurements are shown in Table I.

## D. K-Factor Determination and Uncertainty

The systematic error in the determination of the number of fissions in a sample depends on the accuracy of the K-factors, which were used for normalization in both analytical methods. Here we describe how the K-factors were obtained and provide information on their accuracy. Since the K-factor for <sup>99</sup>Mo is considered to be the most accurate and has been subjected to the greatest number of checks, its determination is described in detail.

The K-factor for <sup>99</sup>Mo was determined using a facility (described in Ref. 15) normally used for assay of fissionable materials by comparison fission counting. The facility consists of a double fission counter inserted in a cavity in the graphite thermal column of a reactor. Two foils are placed back-to-back and simultaneously counted in the same neutron flux.

To determine the K-factor, a <sup>235</sup>U sample was irradiated between two <sup>235</sup>U standard foils in the

**TABLE I**  
**DETERMINATION OF THE NUMBER OF FISSIONS**  
**FOR SAMPLES 1, 2, AND 3**

Fission Product	Analytical Technique	Number of Determinations or Spectra	Sample 1		Sample 2		Sample 3	
			Precision (1 $\sigma$ in %)	Number of Fissions	Precision (1 $\sigma$ in %)	Number of Fissions	Precision (1 $\sigma$ in %)	Number of Fissions
<sup>99</sup> Mo	RC and $\beta$ ctg	4 det	0.62	$4.736 \times 10^{10}$	0.24	$4.925 \times 10^{10}$	0.47	$4.711 \times 10^{10}$
<sup>140</sup> Ba	RC and $\beta$ ctg	2 det	0.75	$4.768 \times 10^{10}$	0.85	$4.889 \times 10^{10}$	0.30	$4.679 \times 10^{10}$
<sup>90</sup> Zr	Ge(Li) $\gamma$ ctg	6 spec	0.9	$4.786 \times 10^{10}$	0.87	$5.012 \times 10^{10}$	1.06	$4.843 \times 10^{10}$
<sup>99</sup> Mo	Ge(Li) $\gamma$ ctg	6 spec	1.1	$4.757 \times 10^{10}$	1.24	$4.952 \times 10^{10}$	1.14	$4.799 \times 10^{10}$
<sup>140</sup> Ba-La	Ge(Li) $\gamma$ ctg	6 spec	0.4	$4.744 \times 10^{10}$	0.43	$4.981 \times 10^{10}$	0.46	$4.752 \times 10^{10}$
<sup>141</sup> Ce	Ge(Li) $\gamma$ ctg	6 spec	1.5	$4.755 \times 10^{10}$	1.29	$5.005 \times 10^{10}$	1.45	$4.730 \times 10^{10}$
<sup>147</sup> Nd	Ge(Li) $\gamma$ ctg	6 spec	1.9	$4.689 \times 10^{10}$	1.91	$4.883 \times 10^{10}$	2.3	$4.857 \times 10^{10}$
		Weighted Average		$4.750 \times 10^{10}$		$4.941 \times 10^{10}$		$4.714 \times 10^{10}$
		Precision of Average	0.27%			0.26%		0.38%

double fission counter. The number of fissions per unit weight in the sample was taken to be the average of those in the standard foils on either side of it. Flux-depression and self-shielding effects were estimated to be negligible for the sample size ( $\approx 2$  mg) and geometry used for the irradiation.

The sample was then dissolved, and multiple specimens obtained from it were separated and the <sup>99</sup>Mo beta activity was counted in a special proportional counter reserved for this purpose. The ratios of the weights of the two standard foils to the weight of the original sample were determined by preparing a new foil from the sample solution and counting it together with each of the standard foils in the double fission chamber. The fraction of the original solution on the new foil was obtained by tracing with <sup>232</sup>U, using a carrier-free procedure. Since the specific alpha activity for <sup>232</sup>U is  $\approx 10^7$  times higher than for <sup>235</sup>U, alpha counting of the tracer provided an accurate method of determining the yield of the electrodeposition procedure used in preparing the new foil.

The K-factor was obtained from the observed <sup>99</sup>Mo beta counting rate, the number of fissions counted on the standard foils during the irradiation, and the ratio of the weight of the sample to the weights of the standard foils. An advantage of the K-factor method is that it is determined directly by fission counting and therefore does not require a knowledge of fission-product yields or decay schemes.

The normalization of the gamma-counting results was based on the K-factor for <sup>99</sup>Mo. The K-factor for <sup>140</sup>Ba was determined separately, then checked against the factor for <sup>99</sup>Mo.

One source of uncertainty in the <sup>99</sup>Mo K-factor was the determination of the number of fissions in the standard foils. The statistical uncertainty calculated from the number of counts was 0.2%. Actual fission-counting data from the two foils counted in the equipment checkout procedure on 152 different days over a 4-yr period had a standard deviation of 0.17%, which is consistent with the estimated value.

The standard foils consisted of 0.1  $\mu\text{g}$  <sup>235</sup>U deposited on an area of 3.8 cm<sup>2</sup>. It is estimated that, under the conditions of the measurement, all but 2% of the fissions produced pulses that were detected. The 2% correction is believed to be known to 10% of its value, thus giving an overall uncertainty in the correction of 0.2%.

According to Ref. 15, the standard deviation of the amount of <sup>235</sup>U determined to be on another foil by comparison fission counting with a traced standard is 0.46%, and that for a solution assayed by this method it is 0.55%. We used 0.55% as the uncertainty in determining the ratio of the weights of the standard foils to that of the sample.

A final source of uncertainty is in the separation and counting of the <sup>99</sup>Mo activity. The average standard deviation of a single <sup>99</sup>Mo separation and counting was determined to be 0.96%, based on a



study of 348 duplicate or multiple analyses over a 3-yr period.<sup>16</sup> In the original evaluation of the K-factor in current use, six analyses for <sup>99</sup>Mo were carried out. The standard deviation of the mean would be expected to be  $0.96\%/\sqrt{6} = 0.39\%$ .

All of the above uncertainties are uncorrelated; it is therefore legitimate to take the overall standard deviation to be the square root of the sum of the squares of the individual standard deviations. This gives

$$\sigma_{K\text{-factor}} = (0.2^2 + 0.2^2 + 0.55^2 + 0.39^2)^{1/2} = 0.73\%.$$

We will use  $\sigma = 0.8\%$  as the systematic error in the determination of the number of fissions.

The K-factor for <sup>99</sup>Mo in current use at LASL was determined in 1955 using a single bombardment and six individual <sup>99</sup>Mo assays. Since then there have been 6 additional bombardments and 15 individual assays. A K-factor based on all 21 assays differs from the original value by 0.4%, which is well within the assigned uncertainty of 0.8%.

In another check on the accuracy of fission determinations using the K-factor method with <sup>99</sup>Mo, LASL and the Lawrence Livermore Laboratory (LLL) have determined the number of fissions in duplicate samples 13 times over the past 11 yr.<sup>17</sup> The average ratio of the LASL to the LLL determinations is 1.007, which is also consistent with an uncertainty of 0.8%.

#### E. Interlaboratory Comparison of Fission Determinations

In connection with the current decay heat studies sponsored by the NRC, LASL prepared duplicate samples of irradiated <sup>235</sup>U that were analyzed at LASL, the Oak Ridge National Laboratory (ORNL), and the Idaho National Engineering Laboratory (INEL). Details of this comparison are given in the Appendix, which was prepared by R. G. Helmer and R. L. Heath of the INEL.

Results of the comparisons are summarized in Table II. The good agreement among the fission determinations by the three Laboratories indicates that our fission determinations are free of unrecognized systematic error.

TABLE II  
RESULTS OF INTERLABORATORY  
COMPARISON OF FISSION  
DETERMINATIONS

Laboratory	Fissions per ml of Standard Solution	Relative Number of Fissions per ml
LASL	$(1.179 \pm 0.009) \times 10^{10}$	1.000
INEL	$(1.176 \pm 0.026) \times 10^{10}$	0.997
ORNL	$(1.184 \pm 0.018) \times 10^{10}$	1.004

#### IV. GAMMA LEAKAGE CORRECTION

Some of the gamma component of the decay heat penetrates the copper absorber block, and is not recorded by the calorimeter. On the other hand, < 0.01% of the beta energy is lost. The gamma energy that escapes must be evaluated separately and added to that deposited in the calorimeter to obtain the total decay heat. Our procedure was to determine experimentally the absolute gamma spectra emitted by the sample for several cooling times, and then to calculate the fractions of these spectra that had escaped the copper block.

#### A. Measurements of Gamma Spectra

Figure 8 shows a plan view of the spectrometer used to measure the absolute gamma spectra at 10 cooling times following a  $2 \times 10^4$  s thermal-neutron irradiation of a thin <sup>235</sup>U sample. This spectrometer was developed for measuring neutron-capture gamma ray spectra. The aluminum-clad <sup>235</sup>U sample was located in an evacuated bismuth-lined channel that passed transversely through the reactor's graphite thermal column and extended into the concrete shielding beyond the graphite. Because there was no thermal column graphite directly behind the sample, this important source of background was eliminated. Gamma rays from the

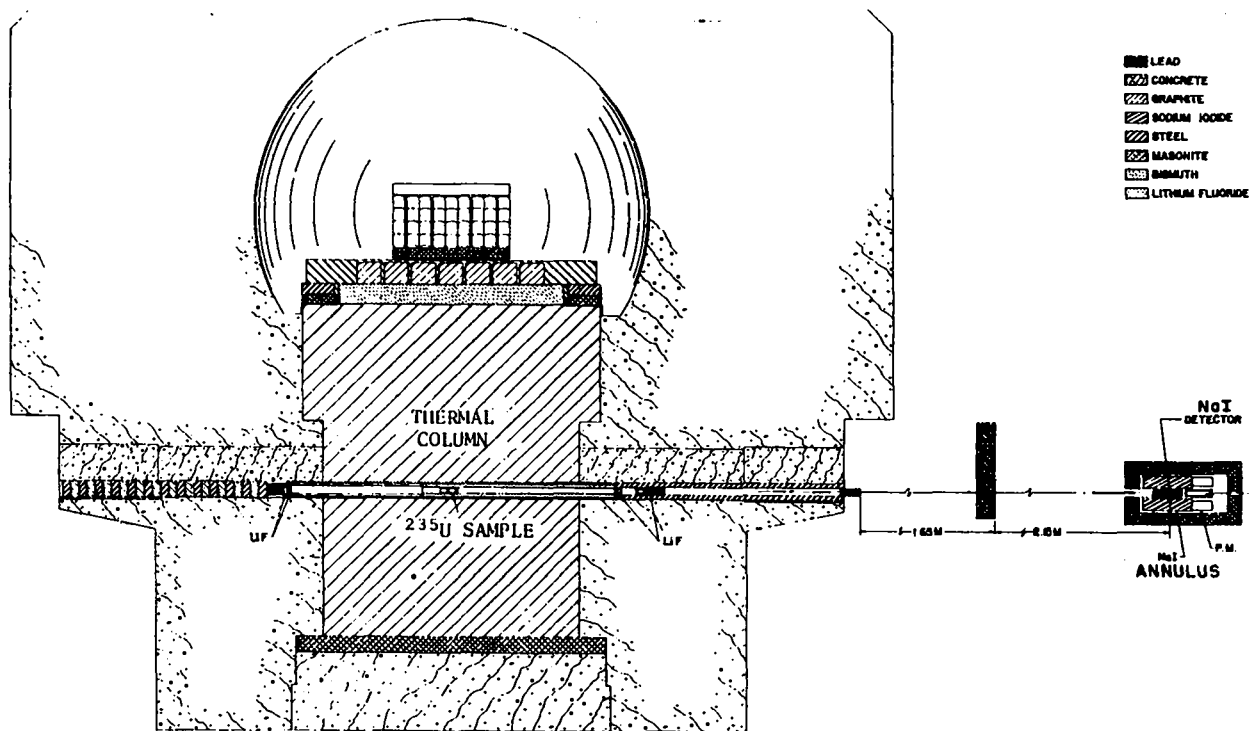


Fig. 8.

Plan view of spectrometer used to measure  $^{235}\text{U}$  fission-product gamma spectra at various cooling times following a  $2 \times 10^4$  s irradiation. The spectra were put on an absolute basis by calibration against hydrogen neutron-capture gammas from a polyethylene sample irradiated in the same flux and position as the  $^{235}\text{U}$  sample.

reactor core were attenuated on entering the thermal column by a 76-mm-thick lead shield adjacent to the core and by a 127-mm-thick bismuth shield just inside the thermal column. The thermal neutron flux at the target was  $\approx 3 \times 10^{11}$  n/cm<sup>2</sup>s. The gamma-ray beam was extracted through a collimator, whose viewing area did not include the bismuth walls of the channel. Therefore, to pass through the collimator, any gamma rays that did not originate in the sample had to scatter through a large angle. Thermal neutrons accompanying the gamma-ray beam during irradiation of standard polyethylene calibration samples were attenuated by a  $^6\text{LiF}$  absorber, which also stopped beta rays from reaching the detector.

The detector was a 61-mm-diam by 127-mm-deep NaI(Tl) crystal placed at the center of a 200-mm-o.d. by 300-mm-deep cylindrical NaI(Tl) annulus, which had a 63.5-mm bore along its axis. The outer crystal was used in anticoincidence with the center

crystal. The gamma-ray beam was 12 mm in diameter at the detector, approximately 6 m from the sample. The data were recorded in a 4096-channel pulse-height analyzer, and read out onto magnetic tape for computer analysis.

A fission counter near the sample position monitored the neutron flux and a nearby fission chamber was used to control the reactor power during irradiations so that the flux at the sample position remained constant.

Before irradiating a  $^{235}\text{U}$  sample, a standard polyethylene sample was irradiated and the single gamma ray of  $E_H = 2.2246 \pm 0.0001$  MeV (Ref. 18), resulting from neutron capture in hydrogen, was recorded by the spectrometer for a convenient time,  $\Delta t$ . The number of hydrogen atoms in the sample [composition  $(\text{CH}_2)_n$ ] was determined by weighing.

The  $^{235}\text{U}$  sample, which was also weighed before being sealed in an aluminum envelope, was then irradiated for  $2 \times 10^4$  s, after which the reactor was

rapidly shut down. (This reduced the thermal flux by a factor of  $10^6$ , and effectively ended the irradiation.)

The gamma power per unit fission rate  $\Gamma(E,t)$  per unit energy interval about  $E$  is given at cooling time  $t$  by

$$\Gamma(E,t) = E_H \frac{G_{\text{det}}(E,t) f(E_H) N_H \sigma_H(n,\gamma)}{G_{\text{det}}(E_H) f(E) N_U \sigma_U(\text{fission})}$$

where  $G_{\text{det}}(E_H)$  is the gamma power recorded by the spectrometer for the hydrogen capture line, and  $G_{\text{det}}(E,t)$  is the gamma power recorded at cooling time  $t$  in the unit energy interval about  $E$ . The function  $f(E)$  is the relative efficiency of the spectrometer at energy  $E$ .  $N_H$  and  $N_U$  are the number of hydrogen and uranium atoms, respectively, and  $\sigma_H(n,\gamma)$  is the capture cross section of hydrogen and  $\sigma_U(\text{fiss})$  is the thermal fission cross section of uranium. The above equation assumes that the thermal neutron flux was the same during the  $^{235}\text{U}$  irradiation as it was during the polyethylene irradiation.

The relative efficiency  $f(E)$  of the spectrometer at energy  $E$  applies to the full-energy peak of the incident gamma ray. However, a single gamma ray of energy  $E$  contributes to the counting rate at all energies below the full-energy peak. Before applying the above equation for  $\Gamma(E,t)$ , it is necessary to "unfold" the observed spectrum to remove the low-energy part of the response function. The unfolding was done by a stripping process starting at the high end of the spectrum. Account is taken of the following processes that occur in the NaI(Tl) crystal: (1) a Gaussian-shaped full-energy peak at the energy of the gamma ray, (2) electron bremsstrahlung, which at high energies broadens the distribution on the low-energy side of the peak, (3) the Compton scattering contribution, which is treated as independent of energy and is subtracted from the remaining spectrum at energies below the peak, and (4) the first and second pair-production escape peaks, which occur at 511 and 1022 keV below the gamma-ray energy.

Figure 9 shows the spectrometer response to the single  $(n,\gamma)$  hydrogen gamma ray at 2.2246 MeV. The ratio of the area under the peak to the total area is 0.64 for the hydrogen gamma ray. This ratio varies from  $\approx 0.95$  for very low energy gamma rays to  $\approx 0.5$

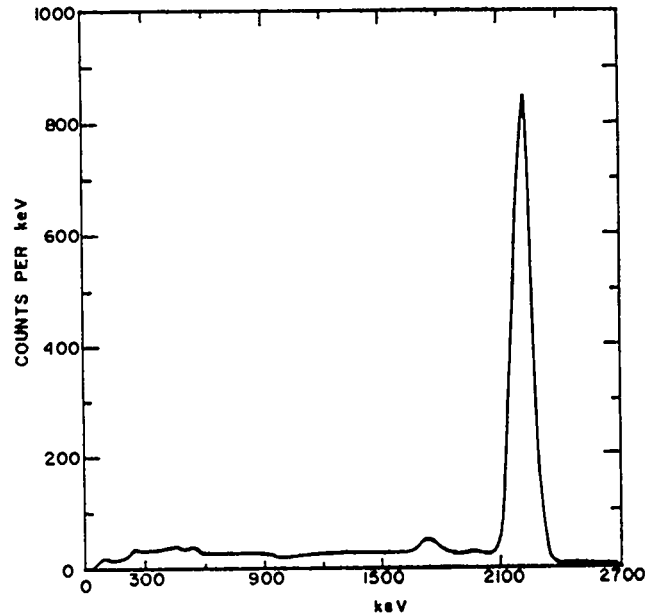


Fig. 9.

*Pulse height spectrum from the single hydrogen neutron-capture gamma ray at  $E_H = 2224.6$  keV. The first pair-production escape peak is visible at 1714 keV.*

at 10 MeV. The large fraction of the recorded energy in the full-energy peak results from the use of a well-collimated gamma-ray beam incident on the center of the end of the central NaI(Tl) crystal and an anticoincidence annulus around the central counter. This response curve feature makes the use of a simple stripping procedure for the unfolding process practical.

In addition to the statistical uncertainty calculated for sample and background, the unfolding process was assigned an RMS uncertainty of  $\pm 10\%$ , which was included in calculating the total uncertainty of the gamma power from fission products.

Gamma spectra at 10 cooling times following a  $2 \times 10^4$  s thermal-neutron irradiation of a  $^{235}\text{U}$  sample are shown in Figs. 10 through 19. The data are combined into 50-keV energy bins. All experimental points are absolute, except for those shown in Fig. 19, which were normalized to a summation calculation because difficulties in background subtraction precluded the determination of accurate absolute

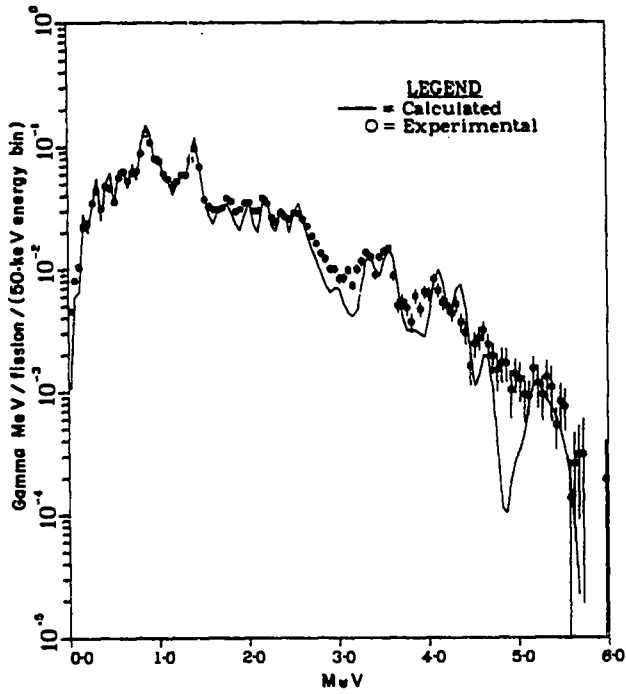


Fig. 10.  
Gamma spectrum for 70-s mean cooling time.

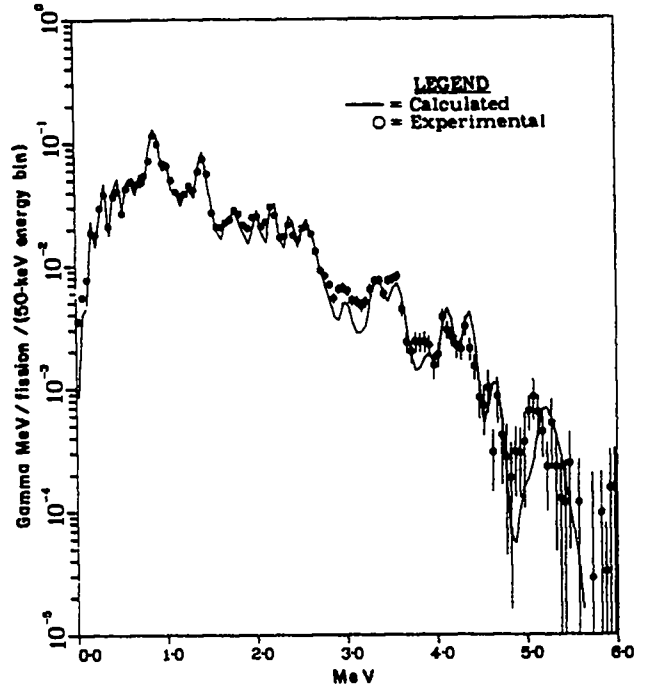


Fig. 11.  
Gamma spectrum for 199-s mean cooling time.

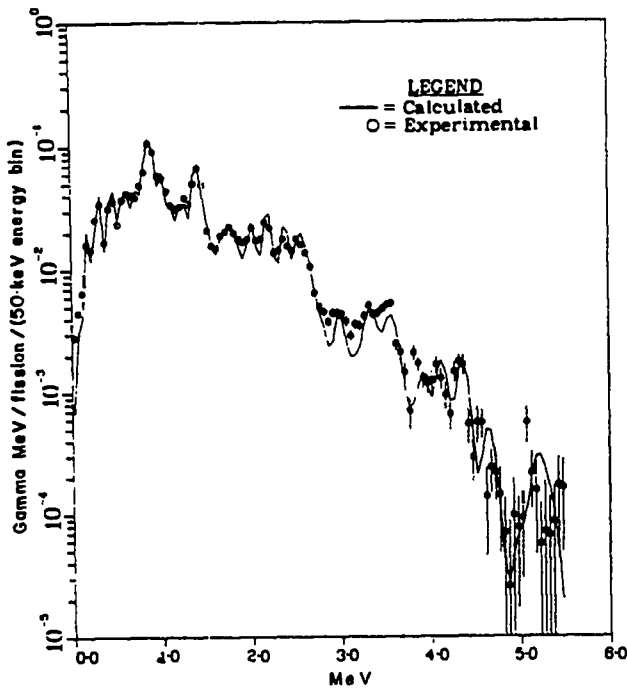


Fig. 12.  
Gamma spectrum for 388-s mean cooling time.

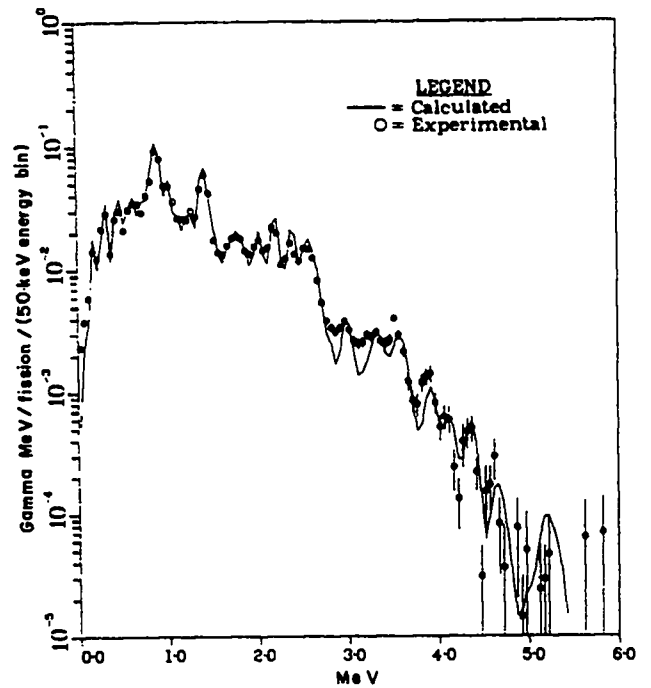


Fig. 13.  
Gamma spectrum for 660-s mean cooling time.

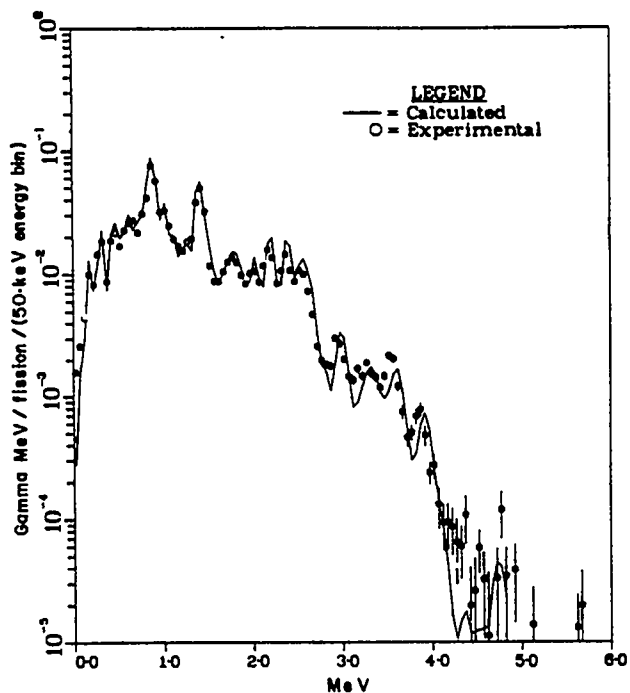


Fig. 14.

Gamma spectrum for 1524-s mean cooling time.

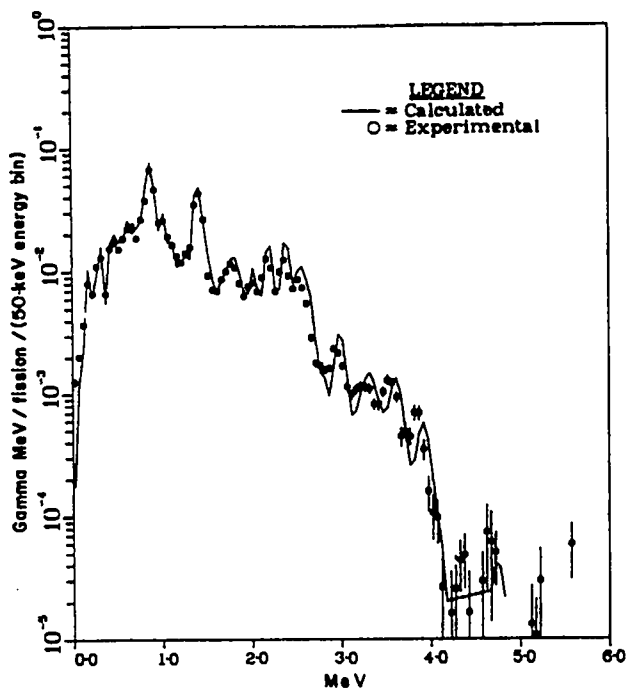


Fig. 15.

Gamma spectrum for 2214-s mean cooling time.

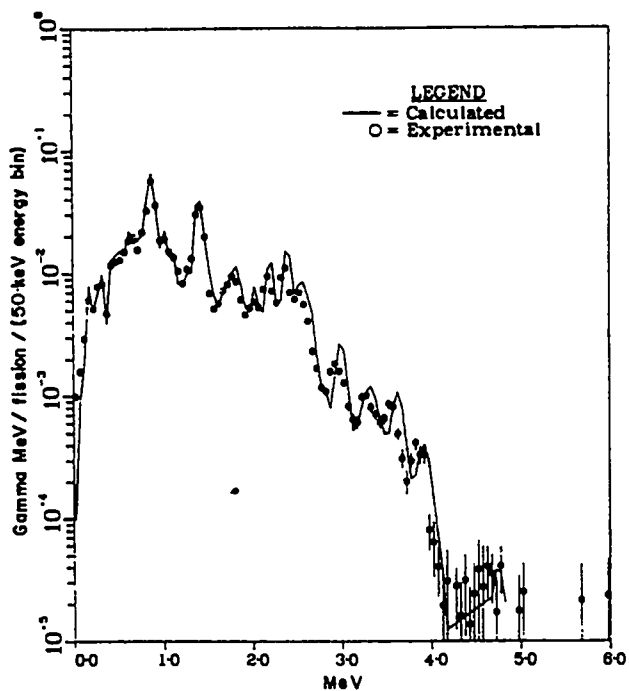


Fig. 16.

Gamma spectrum for 3234-s mean cooling time.

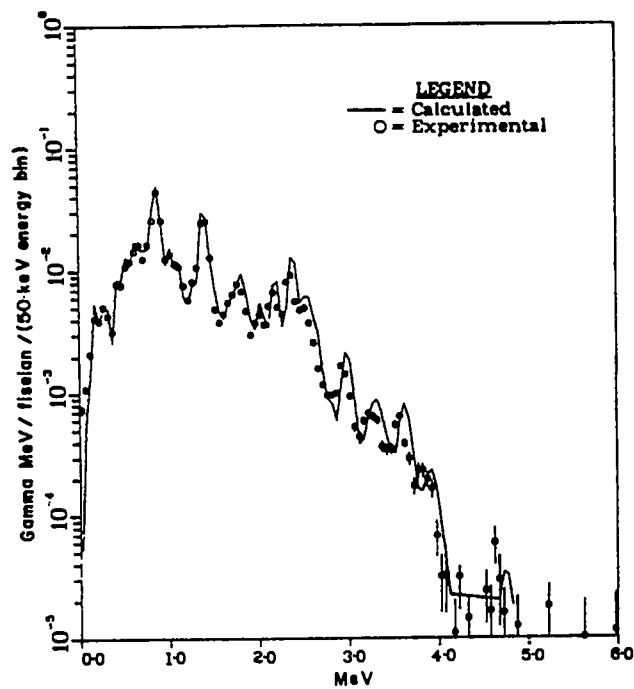


Fig. 17.

Gamma spectrum for 5000-s mean cooling time.

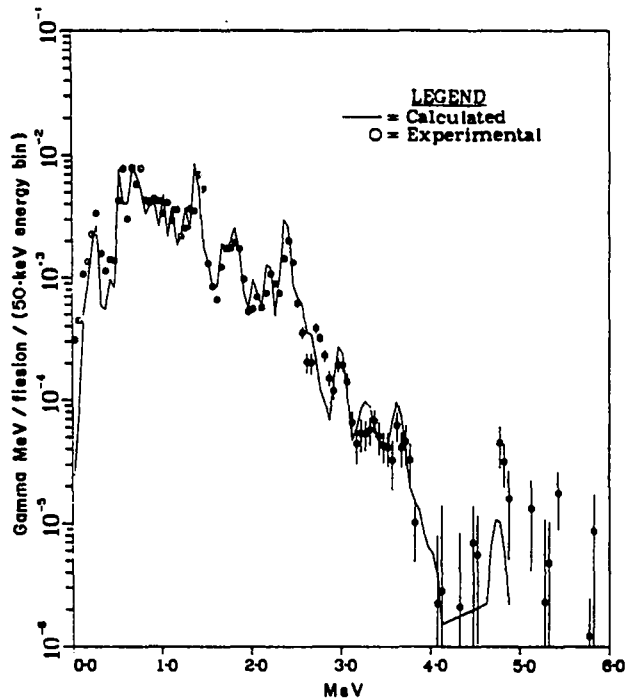


Fig. 18.

Gamma spectrum for 21 845-s mean cooling time.

values. However, earlier results from a pilot experiment indicate that the absolute experimental spectra in this range of cooling times were within  $\approx 10\%$  of the calculated values.

Also shown are spectra calculated at the same cooling times from ENDF/B-IV data.<sup>19</sup> The shapes of the spectra were obtained from the 181 fission products whose files contain spectra. These spectra were normalized to the total gamma release rate for all 711 radioactive species in the files, then broadened to match the experimental energy resolution. Table III gives the experimental integrated gamma decay heat, the ratios of experimental to calculated values, and the percentage of the calculated gamma energy that is due to the 181 nuclides with known spectra.

## B. Calculation of the Gamma Energy Leakage

The gamma-ray leakage calculations were performed using the Monte Carlo gamma-ray transport code MCG.<sup>20</sup> The geometric model included all of the detail shown in Fig. 20. Since the

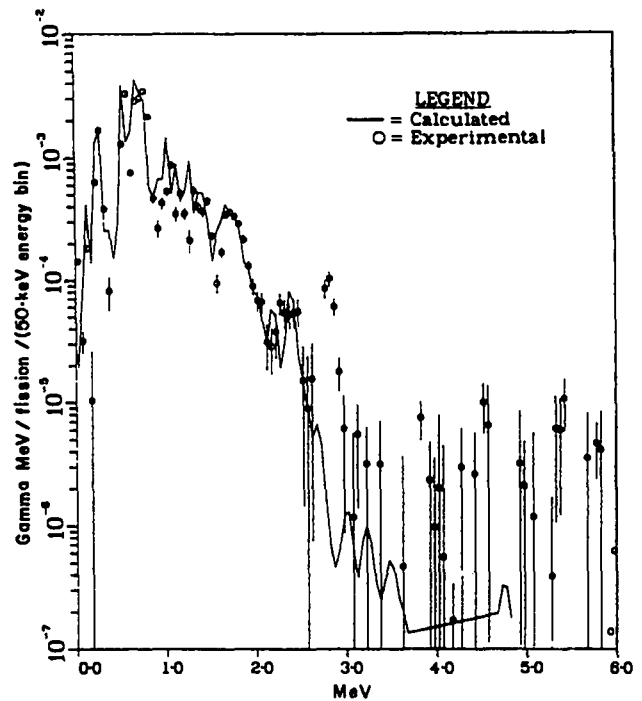


Fig. 19.

Gamma spectrum for 72 550-s mean cooling time. For this cooling time only, the experimental data were normalized to the calculated gamma decay heat because of difficulties in background subtraction. However, preliminary measurements in this region of cooling time were within  $\approx 10\%$  of the calculations.

fission-product gamma-ray energy spectrum varies with cooling time, it was necessary to calculate the energy leakage  $L(E)$  as a function of gamma-ray source energy  $E$ . Approximately 50 000 gamma-ray histories were tracked for each of 17 source energies from 0.1 to 10 MeV. The results given in Table IV and Fig. 21 are for those cases where  $L(E)$  exceeded 0.5% of  $E$ . In all cases, the Monte Carlo statistical uncertainty in  $L(E)$  is  $< 0.2\%$  of  $E$ . From direct experimentation with different geometric models, we estimate that the uncertainty in  $L(E)$  due to the model is  $\sim 0.3\%$  of  $E$ . For most cases of interest, uncertainty in  $L(E)$  is less important than the uncertainty in the source energy spectrum.

Combining the measured source spectra with the calculated leakage fractions gives the total gamma energy leaking from the calorimeter block, on an absolute basis, as shown in Fig. 22. Since spectral

TABLE III

INTEGRATED GAMMA DECAY HEAT

Mean Cooling Time (s)	Experimental Gamma Decay Heat (MeV/fiss)	Ratio Exp/Calc Gamma Decay Heat	Percentage of Calc Gamma Decay Heat from Nuclides Having Spectral Data
70	2.927	1.078 (1.080) <sup>a</sup>	87.6
199	2.198	1.066 (1.069)	93.5
388	1.841	1.068 (1.071)	95.5
660	1.526	1.029 (1.032)	96.6
1524	1.090	0.992 (0.995)	99.8
2214	0.8995	0.979 (0.983)	98.7
3234	0.7168	0.971 (0.976)	99.3
5000	0.5320	0.975 (0.981)	99.7
21 845	0.1418	1.106 (1.121)	99.8
72 550	0.0350 (calculated)		

<sup>a</sup>For the ratios in parentheses, the internal conversion energy has been excluded from the calculated gamma decay heat (for the 38 nuclides having internal conversion coefficients in the ENDF/B-IV files). Internally converted gamma rays would not be detected by the gamma spectrometer used to obtain the experimental gamma decay heat.

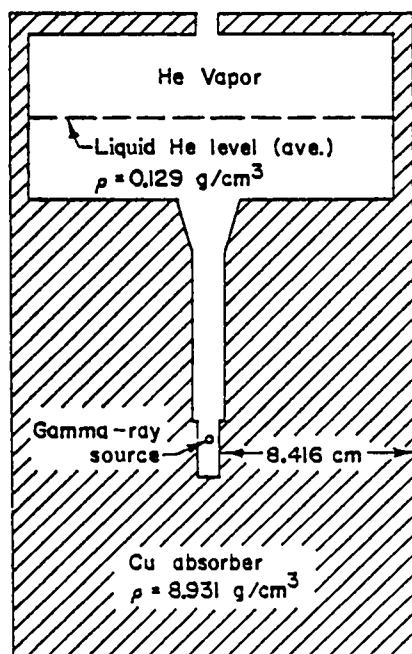


Fig. 20.

Geometric representation of the absorber block used in the Monte Carlo gamma-ray leakage calculations.

TABLE IV

ENERGY DEPENDENCE OF GAMMA-RAY LEAKAGE

Energy (E) (MeV)	Energy Leakage/Source Energy [L(E)/E]
0.4217	0.0056
0.5623	0.0108
0.7499	0.0196
1.000	0.0320
1.334	0.0506
1.778	0.0728
2.371	0.0946
3.162	0.1108
4.217	0.1217
5.623	0.1231
7.499	0.1197
10.00	0.1056

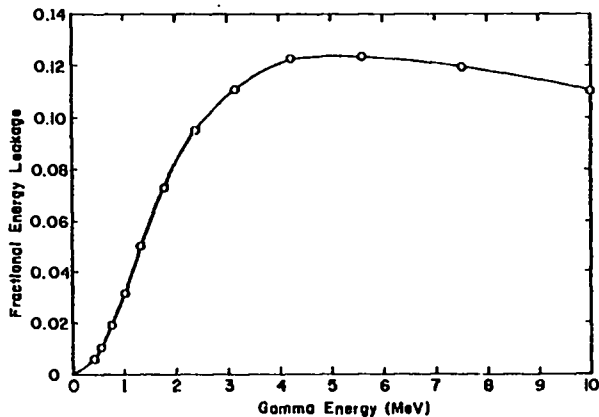


Fig. 21.

Fractional gamma energy leakage from the copper block in the calorimeter as a function of initial gamma energy. These data, obtained using the Monte Carlo code MCG, were combined with the measured spectra to obtain the gamma leakage correction.

measurements were not made at cooling times  $< 70$  s, the average of calculations made with two other spectra was used as a guide in extrapolating the gamma energy leakage to 10 s. The first spectrum, measured by Dickens et al.,<sup>21</sup> was from a  $^{235}\text{U}$  sample irradiated for 100 s, cooled for 100 s, and counted for 50 s. Because of the short irradiation time, the Dickens et al. spectrum is expected to be harder than would be obtained for a 20 000-s irradiation time. The second spectrum was calculated using the ENDF/B-IV nuclear data file; this spectrum might be softer than the true spectrum because of the omission of (unknown) high-energy gammas with short decay times. The energy leakage calculated from the two spectra differed by 15%. The average leakage fraction for the two spectra was used at 10 s, and the absolute energy leakage was obtained from (1) the average leakage fraction, (2) the fraction of the total decay heat that is in the form of gamma radiation (obtained from summation calculations), and (3) the decay heat measured by the calorimeter at 10-s cooling time.

The gamma leakage decay heat was added to that measured with the calorimeter to obtain the total decay heat. An interpolation scheme was used to obtain gamma leakage values between cooling times for which it had been determined.

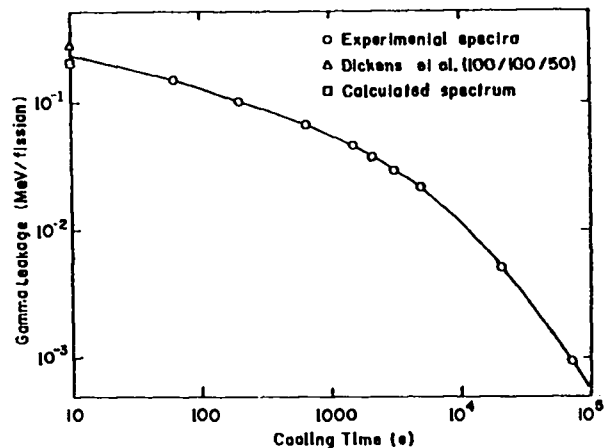


Fig. 22.

Gamma leakage from the calorimeter in absolute units.

The uncertainty in the gamma correction, arising mainly from uncertainties in the spectra, was taken to be 15% of the correction for  $t_{\text{cool}} \leq 15$  s, falling to 10% for  $t_{\text{cool}} \geq 70$  s. Figure 23 shows the gamma correction and its uncertainty, expressed as a percentage of the total decay heat.

## V. CORRECTION FOR INITIAL TRANSIENT

The introduction of the irradiated sample in its aluminum cladding (which was also activated) caused a disturbance to the calorimeter. Also, the finite response time of the system distorted the indicated decay heat curve. Corrections were made to the short-cooling-time data for both of these effects.

Figure 24 shows the initial power recorded by the calorimeter, together with the power recorded when an all-aluminum dummy sample was irradiated and transferred to the calorimeter, using the same mechanism and timing sequence used for the uranium-loaded sample. The initial temperature of the dummy sample was adjusted to be approximately equal to that of the real sample.

To correct for the effects of introducing the sample, the average signal for three irradiated dummy samples was subtracted from the calorimeter power recorded when a uranium-loaded sample was used. This correction amounted to 2.3% at 10 s, and to



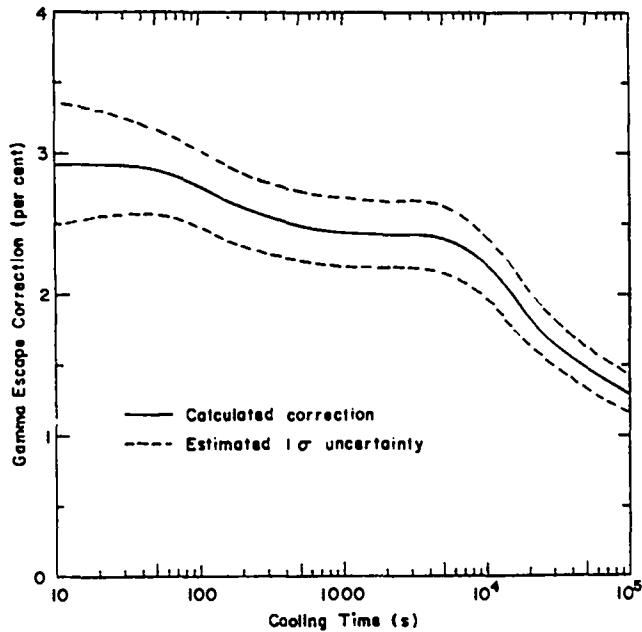


Fig. 23.

Gamma leakage from the calorimeter expressed as a percentage of the total decay heat. The estimated  $1\sigma$  uncertainty band is also shown.

< 0.1% for cooling times > 400 s. The correction includes the effect of the 2.24-m  $^{28}\text{Al}$  activity produced in the aluminum cladding. This activity was estimated to contribute  $\approx 15$  mW at  $t = 0$ .

The calorimeter had an exponential response function with time constant  $R = 0.85$  s. If the true input power is given by

$$P_{\text{in}} = \sum_i \alpha_i e^{-t/\tau_i}$$

where the  $\alpha_i$  and  $\tau_i$  are constants and  $t$  is the time, then the indicated power is given by

$$P_{\text{out}} = \sum_i \frac{\alpha_i (e^{-t/\tau_i} - e^{-t/R})}{(1 - R/\tau_i)}$$

A correction for this effect was obtained by representing the decay heat power (obtained from summation calculations) as a sum of exponentials, as in the equation for  $P_{\text{in}}$ . The correction was obtained by calculating  $P_{\text{in}}/P_{\text{out}}$  as a function of cool-

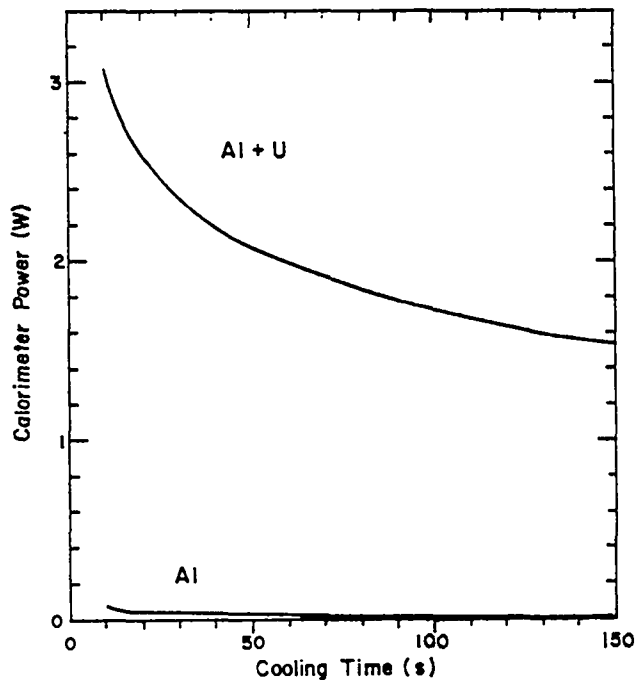


Fig. 24.

Initial power recorded by the calorimeter for an aluminum-clad uranium sample and an aluminum dummy sample.

ing time and multiplying the indicated calorimeter power (after subtraction of the dummy sample background) by this ratio. The correction amounted to 1.1% at a cooling time of 10 s, and to < 0.1% for cooling times > 200 s.

To test these corrections we used a programmed power supply to furnish an exponentially decaying power to the heater in the copper block. The exponential time constant was 47.45 s, which is close to the apparent time constant for the decay heat curve at a cooling time of 6 s.

A dummy sample was irradiated and transferred to the calorimeter in the normal manner. Approximately 1 s after the dummy sample fell into the calorimeter, the exponential power to the heater was started. (The 1-s delay was needed to prevent gas flow due to the heater power from interfering with the fall of the dummy sample into the calorimeter.) This test was carried out twice, and the indicated calorimeter power for the two runs was averaged.

The corrections described above were applied, using the appropriate expression for  $P_{\text{in}}$ . The corrected calorimeter power was then compared to the known

input power. Between 15 and 70 s the average difference between the curves, taken at 1-s intervals, was  $(-0.02 \pm 0.30)\%$ , and the maximum difference was 0.6%. (The minus sign indicates that the calorimeter power was smaller than the input power.) At 10-s cooling time, the calorimeter power was  $\approx 2\%$  below the input power. We feel that the test substantiates the correction technique for cooling times  $\geq 15$  s. Although we are not sure whether the  $\approx 2\%$  discrepancy at 10 s was significant for the decay heat measurements (the small differences in timing could be important at this short cooling time), we made no further adjustment to the experimental data for the 10-s cooling time.

We estimate the uncertainty in the total short-time correction to be  $\approx 50\%$  of its magnitude. This value includes an allowance for the uncertainty at 10 s and is based partly on the results of other methods of estimating the correction (none of which agreed as well with the exponential heating test as the correction actually used).

## VI. DATA TREATMENT AND ERROR ANALYSIS

### A. Data Treatment

The final results are based on experimental runs on three  $^{235}\text{U}$  samples. For most cooling times, data were obtained from all three samples. At certain cooling times, data from fewer than three samples were obtained. The results at 10, 15, 4000, 7000, 25 000, and 30 000 s are based on two samples, and those at 4500, 5000, 62 183, and  $10^5$  s are based on only one sample. Figure 25 shows the individual data points from sample 1 for the first 100 s of cooling time.

The data were smoothed to eliminate fluctuations caused by the boiling process. For times  $\leq 200$  s, the corrected data for each sample were plotted, and a smooth curve was drawn through each set of points. The decay heat was read from the smooth curves at selected cooling times that were an integral number of seconds. (This corrected for the 0.15-s displacement of the centers of the 1-s multiscaler channels.) For cooling times from 200 through 4000 s, the average of ten 1-s channels was used. For times between 4000 and 30 000 s, we took the average for ten

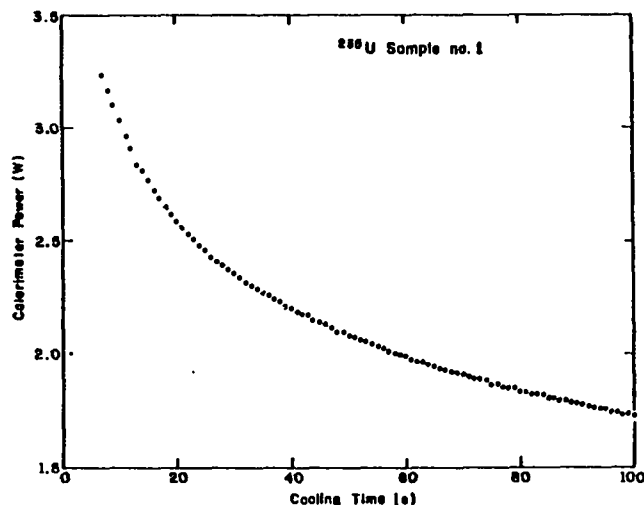


Fig. 25.

Individual data points from a single  $^{235}\text{U}$  sample. Background from an irradiated aluminum dummy sample has been subtracted.

10-s channels; for cooling times  $> 30\ 000$  s, we took the average of 10 timed measurements made with the dry test meter (carried out over a period of  $\approx 30$  m). The smoothing techniques were chosen because they were compatible with the rate of change of the decay heat at the times involved, and they introduced no significant systematic errors in the measurements.

The data for each sample fell on a relatively smooth curve, indicating a high degree of correlation between measurements made at adjacent cooling times. The decay heat curves for the three samples were nearly parallel, although the relative values changed slowly over long intervals of cooling time.

### B. Error Analysis

The RMS scatter in the data at each cooling time was calculated using

$$S = \left( \frac{\sum_i (y_i - \bar{y})^2}{n - 1} \right)^{1/2}$$

where  $y_i$  is an individual data point,  $\bar{y}$  is the mean, and  $n$  is the number of data points. When there were  $< 3$  data points, the missing values were estimated from nearby points on the same curve.

For most cooling times, the RMS scatter in the data was consistent with estimates based on the precision of the fission determination and the scatter of the flowmeter calibration points about the fitted calibration curve. At the shortest cooling times, an increased scatter was observed. This might have been caused by the variation in the time it took for the sample to fall from the release chamber to the copper block, or to some other variation in the initial transient. An increased scatter was also observed for cooling times immediately after the helium reservoir had been refilled for one or more of the runs. This affected the data at cooling times of 6000 and 7000 s.

We can use  $S$  to estimate the statistical uncertainty in the averaged experimental decay heat,  $\bar{y}$ , provided we take account of the small number ( $n = 3$ ) of individual data points that we used in calculating  $S$  and  $\bar{y}$ . If  $n$  had been large, the deviation of  $\bar{y}$  from the true mean,  $m$ , would be normally distributed with a standard deviation of  $s/\sqrt{n}$ . When  $n$  is small,  $(\bar{y} - m)/(S/\sqrt{n})$  has a Student's  $t$  distribution for  $n - 1$  degrees of freedom. This distribution involves greater probabilities of large deviations of  $\bar{y}$  from  $m$  than does the normal distribution.

For simplicity in combining and interpreting uncertainties, we approximate the deviation of  $\bar{y}$  from  $m$  by a normal distribution chosen to have a 95% confidence interval equal to that obtained using the Student's  $t$  distribution. Such a normal distribution has a standard deviation of  $1.3S$ .

Other sources of error, discussed earlier, did not contribute to the scatter in the data from the three samples. For this reason, we call them systematic uncertainties. They were (1) the systematic uncertainty in the fission determination, (2) the uncertainty in the flowmeter calibration, (3) the uncertainty in the gamma-leakage correction, and (4) the uncertainty in the initial-transient correction. We assumed that the errors resulting from these uncertainties were normally distributed and uncorrelated; we therefore equated the total systematic uncertainty,  $\sigma_o$ , to the RMS sum of the individual systematic uncertainties (see Fig. 26).

The total uncertainty,  $\sigma$ , was taken to be the RMS sum of  $\sigma_o$  and  $1.3S$ . Figure 27 shows  $\sigma$ ,  $\sigma_o$ , and  $S$  as functions of cooling time.

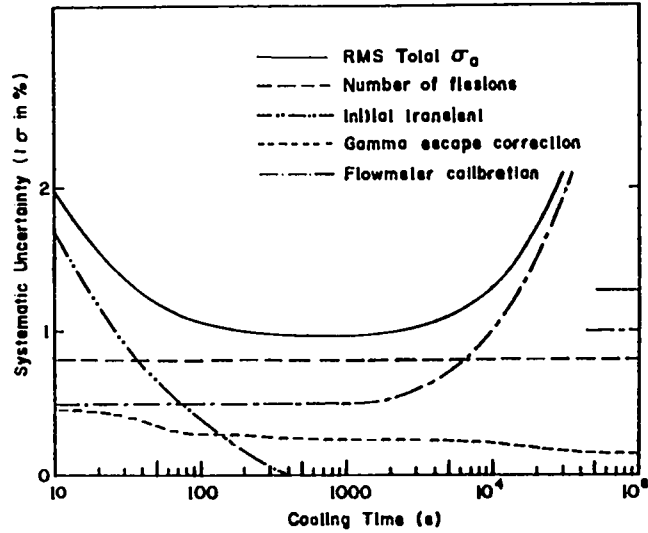


Fig. 26.  
Estimated individual and RMS total systematic uncertainties as functions of cooling time. These uncertainties are the same for all samples.

## VII. RESULTS AND CALCULATIONS

Let  $F(t, T)$  be the decay heat  $t$  seconds after an irradiation of  $T$  seconds at constant fission rate in the absence of neutron capture in fission products. Our experimental data may be written in terms of this function as  $F(t, 2 \times 10^4)$ . To facilitate comparison with the present ANS standard and with the results of others, we extended our data to the infinite-irradiation case (defined as  $T = 10^{18}$  s) using

$$F(t, \infty) = F(t, 2 \times 10^4) + F(t + 2 \times 10^4, \infty) .$$

The second term on the right was obtained using the CINDER-10 summation code<sup>22</sup> with the ENDF/B-IV data base as listed and corrected by England and Schenter.<sup>23</sup> Its contribution to the infinite-irradiation decay heat was 16% at  $t = 10$  s, 51% at  $t = 2500$  s, and 95% at  $t = 10^5$  s. It was assigned an uncertainty of 2%, based on the value estimated by Schmittroth and Schenter<sup>24</sup> for a  $10^7$  s irradiation. This uncertainty was combined quadratically with the experimental uncertainty to obtain the uncertainty for the extended experimental data.

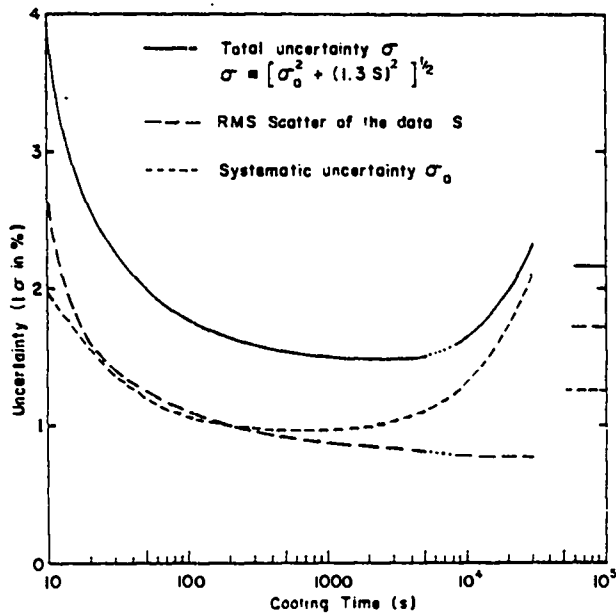


Fig. 27.

Total uncertainty in the data,  $\sigma$ , systematic uncertainty,  $\sigma_0$ , and RMS scatter of the data,  $S$ , at various cooling times. In calculating  $\sigma$ , the value of  $S$  was increased by the factor 1.3 to compensate for a possible underestimate of the true scatter in the data, which results from the small number (3) of data points considered. At 6000- and 7000-s cooling times, where the curves are dotted, the scatter was larger than shown because of the disturbances caused by refilling the calorimeter reservoir with liquid helium. Correct values for  $\sigma$  are given in Table V.

The CINDER-10 code and ENDF/B-IV data base were also used to calculate values of  $F(t, 2 \times 10^4)$  and  $F(t, \infty)$  at cooling times corresponding to those of the experimental data. The experimental results and uncertainties, calculated decay heat values, and the ratios of experiment to calculation are given as functions of  $t$  in Table V.

Figure 28 shows the experimental and calculated decay heats for  $2 \times 10^4$  s irradiations, and Fig. 29 shows their ratio.

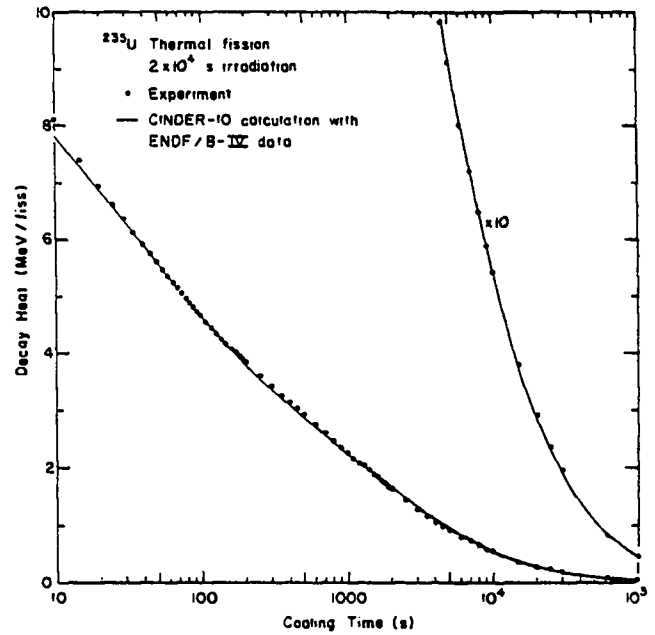


Fig. 28.

Experimental and calculated decay heat for a  $2 \times 10^4$  s irradiation at constant flux.

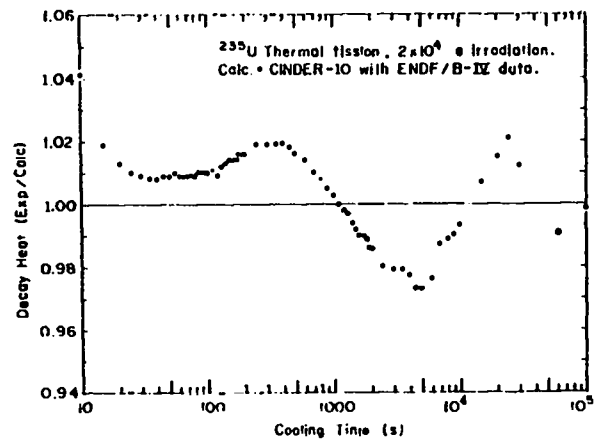


Fig. 29

Ratio of experimental to calculated decay heat for a  $2 \times 10^4$  s irradiation at constant flux.

TABLE V

EXPERIMENTAL AND CALCULATED DECAY HEAT FOR THE PRODUCTS OF THERMAL FISSION OF  $^{235}\text{U}$ 

Cooling Time (s)	$2 \times 10^4$ s Irradiation				Infinite Irradiation			
	Experimental Decay Heat (MeV/fiss)	Experimental Uncertainty (1 $\sigma$ in %)	Calculated Decay Heat using CINDER-10 and ENDF/B-IV (MeV/fiss)	Ratio Exp/Calc Decay Heat	Experimental Decay Heat Extended by CINDER-10 and ENDF/B-IV (MeV/fiss)	Experimental Uncertainty <sup>a</sup> (1 $\sigma$ in %)	Calculated Decay Heat using CINDER-10 and ENDF/B-IV (MeV/fiss)	Ratio Exp/Calc Decay Heat
10	8.10	4.1	7.780	1.041	9.65	3.5	9.327	1.035
15	7.38	3.0	7.239	1.019	8.93	2.5	8.786	1.016
20	6.933	2.6	6.842	1.013	8.480	2.2	8.389	1.011
25	6.595	2.4	6.531	1.010	8.142	2.0		
30	6.335	2.3	6.276	1.009	7.882	1.9		
35	6.109	2.2	6.060	1.008	7.656	1.8		
40	5.920	2.1	5.873	1.008	7.467	1.7	7.420	1.006
45	5.758	2.1	5.709	1.009	7.305	1.7		
50	5.614	2.0	5.562	1.009	7.160	1.6		
55	5.481	2.0	5.429	1.010	7.027	1.6		
60	5.358	2.0	5.309	1.009	6.904	1.6	6.855	1.007
65	5.244	1.9	5.198	1.009	6.790	1.5		
70	5.141	1.9	5.097	1.009	6.687	1.5		
75	5.047	1.9	5.003	1.009	6.593	1.5		
80	4.958	1.8	4.915	1.009	6.504	1.5	6.461	1.007
85	4.881	1.8	4.834	1.010	6.427	1.4		
90	4.806	1.8	4.758	1.010	6.351	1.4		
95	4.734	1.8	4.686	1.010	6.279	1.4		
100	4.667	1.8	4.619	1.010	6.212	1.4	6.164	1.008
110	4.544	1.8	4.496	1.011	6.089	1.4		
120	4.426	1.7	4.385	1.009	5.971	1.4		
130	4.339	1.7	4.286	1.012	5.884	1.4		
140	4.251	1.7	4.195	1.013	5.795	1.4		
150	4.170	1.7	4.112	1.014	5.714	1.4	5.655	1.010
160	4.092	1.7	4.035	1.014	5.636	1.4		
170	4.021	1.7	3.964	1.014	5.565	1.3		
180	3.960	1.7	3.899	1.016	5.503	1.3		
190	3.899	1.6	3.838	1.016	5.442	1.3		
200	3.841	1.6	3.780	1.016	5.384	1.3	5.323	1.011
250	3.608	1.6	3.541	1.019	5.150	1.3		
300	3.419	1.6	3.355	1.019	4.960	1.3		
350	3.265	1.6	3.205	1.019	4.805	1.3		
400	3.135	1.6	3.078	1.019	4.673	1.3	4.616	1.012
450	3.022	1.6	2.969	1.018	4.559	1.3		
500	2.920	1.6	2.873	1.016	4.456	1.3		
600	2.746	1.5	2.709	1.014	4.280	1.2	4.243	1.009
700	2.598	1.5	2.572	1.010	4.130	1.2		
800	2.474	1.5	2.455	1.008	4.004	1.2	3.984	1.005
900	2.363	1.5	2.351	1.005	3.890	1.2		
1000	2.264	1.5	2.256	1.003	3.789	1.2	3.783	1.002

TABLE V (Cont)

Cooling Time (s)	$2 \times 10^4$ s Irradiation				Infinite Irradiation			
	Experimental Decay Heat (MeV/fiss)	Experimental Uncertainty (1 $\sigma$ in %)	Calculated Decay Heat using CINDER-10 and ENDF/B-1V (MeV/fiss)	Ratio Exp/Calc Decay Heat	Experimental Decay Heat Extended by CINDER-10 and ENDF/B-1V (MeV/fiss)	Experimental Uncertainty <sup>a</sup> (1 $\sigma$ in %)	Calculated Decay Heat using CINDER-10 and ENDF/B-1V (MeV/fiss)	Ratio Exp/Calc Decay Heat
1100	2.173	1.5	2.174	1.000	3.696	1.2		
1200	2.093	1.5	2.098	0.998	3.614	1.2		
1300	2.020	1.5	2.027	0.997	3.539	1.2		
1400	1.950	1.5	1.962	0.994	3.467	1.2		
1500	1.886	1.5	1.901	0.992	3.401	1.2	3.416	0.996
1600	1.827	1.5	1.845	0.990	3.340	1.2		
1700	1.773	1.5	1.791	0.990	3.284	1.2		
1800	1.721	1.5	1.741	0.989	3.229	1.2		
1900	1.671	1.5	1.694	0.986	3.177	1.2		
2000	1.627	1.5	1.650	0.986	3.131	1.2	3.154	0.993
2500	1.431	1.5	1.460	0.980	2.925	1.3		
3000	1.283	1.5	1.311	0.979	2.768	1.3		
3500	1.166	1.5	1.191	0.979	2.641	1.3		
4000	1.067	1.5	1.092	0.977	2.533	1.3	2.557	0.991
4500	0.9808	1.5	1.008	0.973	2.438	1.3		
5000	0.9111	1.5	0.9362	0.973	2.360	1.3		
6000	0.7998	2.3	0.8198	0.976	2.231	1.5	2.251	0.991
7000	0.7195	2.0	0.7287	0.987	2.135	1.5		
8000	0.6480	1.6	0.6553	0.989	2.049	1.5	2.056	0.997
9000	0.5886	1.6	0.5948	0.990	1.975	1.5		
10000	0.5401	1.7	0.5440	0.993	1.912	1.5	1.916	0.998
15000	0.3803	1.8	0.3778	1.007	1.691	1.6	1.689	1.001
20000	0.2918	2.0	0.2874	1.015	1.552	1.7	1.547	1.003
25000	0.2359	2.2	0.2311	1.021	1.453	1.7		
30000	0.1947	2.3	0.1923	1.012	1.375	1.7		
62133	0.0823	2.2	0.0832	0.989	1.105	1.9		
100000	0.0454	2.2	0.0455	0.998	0.971	1.9	0.969	1.002

<sup>a</sup>Calculated on the assumptions that the calculated infinite irradiation decay heat curve has 2% uncertainty for  $t_{cool} \geq 2 \times 10^4$  s, and that this uncertainty is uncorrelated with the experimental uncertainty.

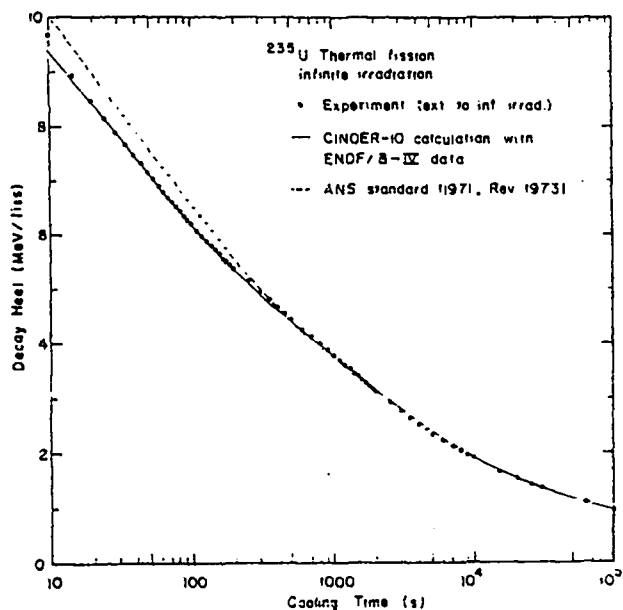


Fig. 30.

Extended experimental data, summation calculations, and present ANS 5.1 Standard for an infinite ( $10^{18}$  s) irradiation at constant flux with no depletion or capture. The ANS Standard plus 20% is currently used in reactor safety evaluations.

Figure 30 compares the extended experimental data, the calculated  $F(t, \infty)$ , and the present ANS Decay Heat Standard. It may be seen that the extended experimental data are in good agreement with  $F(t, \infty)$  calculated from ENDF/B-IV data, and are  $\approx 7\%$  below the ANS standard at short cooling times. Moreover, the experimental uncertainty is significantly smaller than that assigned to the standard.

#### ACKNOWLEDGMENTS

We wish to thank the following for their contributions to this project: E. T. Jurney for measuring the gamma spectra, D. W. Muir for performing the Monte Carlo calculations, G. W. Knobloch and G. W. Butler for determining the number of fissions, T. R. England and M. G. Stamatelatos for making the summation calculations, Steven Koczan and Gilbert Suazo for supervising the hydrogen-furnace

brazing operation on the calorimeter, J. L. Moore for helping to build the apparatus and to carry out the measurements, Frank Newcom for preparing the illustrations, and the OWR personnel for their cooperation and assistance.

We also wish to thank J. K. Dickens, R. G. Helmer, and R. L. Heath for their cooperation in making the fission determination intercomparison.

#### REFERENCES

1. A. M. Perry, F. C. Maienschein, and D. R. Vondy, "Fission-Product Afterheat—A Review of Experiments Pertinent to the Thermal-Neutron Fission of  $^{235}\text{U}$ ," Oak Ridge National Laboratory report ORNL-TM-4197 (October 1973).
2. American Nuclear Society, Draft Standard ANS-5.1, approved by Subcommittee ANS-5 of the ANS Standards Committee, October 1971 (revised 1973).
3. M. Lott, G. Lhiaubet, F. Dufreche, C. Devillers, and R. de Tourveil, "Mesures calorimetriques de la puissance emise par les produits de fission de  $^{235}\text{U}$  pour des temps de refroidissement compris entre 70 secondes et  $7 \times 10^4$  secondes," Bull. Inf. Sci. Tech., Commis. Energ. At. (Fr.) No. 181, pp. 51-59 (May 1973); translation, AEC-TR-7472.
4. Sir James Dewar, *Scientific Uses of Liquid Air* (Proc. R. Inst. G. B., 1894).
5. M. Sklodowska-Curie, "Recherches sur les substances radioactives," 2nd ed. (reviewed and corrected), thesis presented to the Faculty of Sciences, Paris (Gauthier-Villiers, Paris, 1904).
6. J. L. Yarnell and P. J. Bendt, "Fission Product Decay Heat Studies as of December 15, 1975," Los Alamos Scientific Laboratory report LA-6209-SR (January 1976).
7. J. L. Yarnell and P. J. Bendt, "Decay Heat by Calorimetry," in Proc. 4th Water Reactor Safety Information Meeting, Gaithersburg, MD, September 27-30, 1976.

8. F. G. Brickwedde, H. van Dijk, M. Durieux, J. R. Clement, and J. K. Logan, "The 1958 He<sup>4</sup> Scale of Temperatures," *J. Res. Nat. Bur. Stand.* **64A**, 1-17 (1960).
9. E. R. Cohen and J. W. M. DuMond, "Our Knowledge of the Fundamental Constants of Physics and Chemistry in 1965," *Rev. Mod. Phys.* **37**, 537-594 (1965).
10. H. Ter Harmsel, H. van Dijk, and M. Durieux, "The Heat of Vaporization of Helium," *Physica* **36**, 620-636 (1967).
11. L. I. Dana and H. Kamerlingh Onnes, "Further Experiments with Liquid Helium," *Proc. K. Ned. Akad. Wet.* **29**, 1051-1068 (1926).
12. R. Berman and C. F. Mate, "Some Thermal Properties of Helium and Their Relation to the Temperature Scale," *Philos. Mag.* **3**, 461-469 (1958).
13. J. Kleinberg and H. L. Smith, Eds., "Collected Radiochemical Procedures," Los Alamos Scientific Laboratory report LA-1721 (4th ed.) (April 1976).
14. R. Gunnink and J. B. Niday, "Computerized Quantitative Analysis by Gamma-Ray Spectrometry. Vol. I. Description of the GAMANAL Program," Lawrence Livermore Laboratory report UCRL-51061, Vol. I (March 1972).
15. G. W. Knobeloch, "Precision Assay by Fission Counting," presented at Meeting of Central Bureau of Nuclear Measurements, Brussels, November 29-December 2, 1965 (CONF-651112-1).
16. C. I. Browne and K. Halbing, "Standard Deviations of Radiochemical Analyses," Los Alamos Scientific Laboratory report LAMS-2342 (October 1959).
17. G. W. Knobeloch, Los Alamos Scientific Laboratory, private communication, 1976.
18. G. A. Bartholomew, A. Doveika, K. M. Eastwood, S. Monaro, L. V. Groshev, A. M. Demidov, V. I. Pelekhov, and L. L. Sokolovskii, "Compendium of Thermal-Neutron-Capture Gamma-Ray Measurements, Part 1,  $Z \leq 46$ ," *Nucl. Data, Sect. A*, **3** 367-650 (1967).
19. T. R. England and M. G. Stamatelatos, "Beta and Gamma Spectra and Total Decay Energies from Fission Products," *Trans. Am. Nucl. Soc.* **23**, 493-494 (1976); T. R. England and M. G. Stamatelatos, "Multigroup Beta and Gamma Spectra of Individual ENDF/B-IV Fission-Product Nuclides," Los Alamos Scientific Laboratory report LA-NUREG-6622-MS (December 1976).
20. E. D. Cashwell, J. R. Neergaard, C. J. Everett, R. G. Schrandt, W. M. Taylor, and G. D. Turner, "Monte Carlo Photon Codes: MCG and MCP," Los Alamos Scientific Laboratory report LA-5157-MS (March 1973).
21. J. K. Dickens, T. A. Love, J. W. McConnell, J. F. Emery, and R. W. Peelle, "Fission Product Beta and Gamma Energy Release Quarterly Progress Report for July—September 1975," Oak Ridge National Laboratory report ORNL-TM-5156 (November 1975).
22. T. R. England, M. G. Stamatelatos, and N. L. Whittemore, "Decay Heating, Gas Content, and Spectra Calculations for Fission Products," in "Applied Nuclear Data Research and Development, January 1—March 31, 1976," Los Alamos Scientific Laboratory report LA-6472-PR (August 1976), p. 60.
23. T. R. England and R. E. Schenter, "ENDF/B-IV Fission-Product Files: Summary of Major Nuclide Data," Los Alamos Scientific Laboratory report LA-6116-MS (ENDF-223) (October 1975).
24. F. Schmittroth and R. E. Schenter, "Uncertainties in Fission-Product Decay-Heat Calculations," Hanford Engineering Development Laboratory report HEDL-SA-1114 (1976) (accepted by *Nucl. Sci. Eng.*).



## APPENDIX

### INDEPENDENT MEASUREMENT OF NUMBER OF FISSIONS IN LASL $^{235}\text{U}$ SAMPLE

by

R. G. Helmer and R. L. Heath

Idaho National Engineering Laboratory  
EG&G Idaho, Inc.

Two quantities are determined independently in the decay heat measurements of Yarnell and Bendt<sup>1</sup> and Dickens.<sup>2</sup> These are the decay energy release rate and the fissions rate in the irradiated  $^{235}\text{U}$  samples. In this summary the results are given for an independent determination of the number of fissions in these samples. This work was carried out at the INEL and provides support for the results in these reports. It should be emphasized that the results at LASL and INEL are completely independent due to the different methods used. The two methods used at ORNL are, in part, related to the methods at both LASL and INEL.

The following intercomparison of the measurements of the number of fissions has been carried out. A 63-mg sample of enriched  $^{235}\text{U}$  (93%) was irradiated for 29 s in a thermal flux in the Omega West Reactor at LASL. Except for its duration, this irradiation was the same as the irradiations for the LASL decay heat measurements. The uranium sample was dissolved and diluted to 1 liter. Samples from this solution with volumes of 10.0 ml were shipped to ORNL and the INEL for analysis. A portion of the solution also was analyzed at LASL by the methods used for the decay heat samples and described in Sec. III.B of Ref. 1.

At the INEL the 10-ml sample was completely transferred, a small amount at a time, to a small piece of filter paper and dried. The gamma-ray spectrum of this sample was measured in a standard geometry (at a 10-cm source-detector distance) on a Ge(Li) detector. The determination of the efficiency for the detection of gamma rays and the data analysis methods have been described in Refs. 3 and

4. Four spectra were obtained. In order to determine the number of fissions in this sample, our method required a knowledge of (1) the absolute gamma-ray intensity, or branching ratio, for each gamma ray used, (2) the half-life for each isotope, and (3) the fission yield from thermal fission of  $^{235}\text{U}$ . The relationship is

$$N = \frac{A}{E \cdot B \cdot Y} \frac{e^{\lambda T}}{1 - e^{-\lambda T}},$$

where

- N = number of fissions,
- E = detection efficiency for full-energy peak,
- A = area of full-energy peak for a gamma ray,
- B = gamma-ray branching ratio,
- T = count duration,
- $\tau$  = decay time,
- Y = fission yield, and
- $\lambda = \ln 2/T_{1/2}$ , where  $T_{1/2}$  = half-life.

The decay scheme parameters,  $T_{1/2}$  and B, and fission yields used in this analysis are given in Table A-I. Over the past several years we have been involved in the Interlaboratory LMFBR Reaction Rate (ILRR) Program. As part of this effort we have provided an evaluation of decay scheme parameters for these fission product isotopes. The values in Table A-I are from the latest evaluation;<sup>6</sup> previous evaluations for the ILRR Program are given in Refs. 6 and 7. The uncertainties quoted in the table are 68% confidence level (1  $\sigma$ ) values.

TABLE A-I

## PARAMETERS OF FISSION PRODUCT ISOTOPES FOR INEL ANALYSES

Parameter	<sup>90</sup> Zr	<sup>103</sup> Ru	<sup>140</sup> Ba- <sup>140</sup> La
Half-life (days) <sup>5</sup>	64.1 ± 0.3	39.43 ± 0.10	12.789 ± 0.006
Gamma-ray energy (keV)	724.2 756.7	497.1	1596.2
Branching ratio (%) <sup>5</sup>	44.1 ± 0.5 54.6 ± 0.5	89 ± 1	95.40 ± 0.08
Fission yield (%)			
ILRR <sup>6</sup>	6.52 ± 0.13	3.02 ± 0.06	6.22 ± 0.12
Meek and Rider <sup>9</sup>	6.44 ± 0.09	3.15 ± 0.06	6.29 ± 0.09

The ILRR Program has also involved an interlaboratory comparison of absolute gamma-ray intensity measurements. In Ref. 3 (Tables VI and VII) counting results are given for similar samples from our Laboratory and groups at Argonne National Laboratory, Hanford Engineering Development Laboratory, and Atlantic Richfield Hanford Company. In essentially all cases, the results agree within the quoted uncertainties, which are about 2%. This provides verification of our counting methods.

Two sets of thermal neutron fission yields, in Table A-I, have been used with the results of our gamma-ray counting. The first set consists of measured values from the ILRR Program<sup>6</sup> and the second set is the evaluated values proposed by Meek and Rider<sup>9</sup> for inclusion in the ENDF/B-V data file. As proposed for the ENDF/B file the latter yields have associated codes which indicate a range of uncertainties. The errors in Table A-I are the maximum values for the ranges quoted. The uncertainties for the ILRR yields include only the contribution from the fission rates per atom of <sup>235</sup>U. These errors are larger than that of the K-factor quoted in Sec. III.D of Ref. 1 because they must relate to a known mass of <sup>235</sup>U in the fission chamber, whereas the K-factor depends only on a mass ratio. The other components of the error in the final ILRR fission yields are not included here, since they also occur in our counting results and will be accounted for there.

The results from our counting experiments are given in Table A-II for each set of fission yields. The only significant difference is in the value from <sup>103</sup>Ru

which varies by 4% causing the averages to differ by 1%. The results with the ILRR yields are more consistent; their spread is 2% compared to 4% with the Meek and Rider values. This might be expected since the ILRR yields are from counting experiments similar to this one. The averages in Table A-II are weighted averages.

The various contributions to the uncertainties in Table A-II are listed in Table A-III. The uncertainties in Table A-II for the individual gamma rays included the contributions in Table A-III except for the fission yield errors. We have thus assumed that the yield values are correlated; this is exactly the case for the ILRR yields. The fission yield error, 2.0% for ILRR and an average of 1.6% for the Meek and Rider values, is included in quadrature in the last entry of Table A-II. Since the same gamma-ray branching ratios were used in measuring the ILRR fission yields and in our data analysis, this error cancels and is not included when the ILRR yields are used.

The results of the LASL analysis of samples from the same solution are shown in Table A-IV. The final table entry includes a systematic error of 0.73%, from Sec. III.D of Ref. 1, in addition to the precision error in the weighted average.

As can be seen, the LASL result of  $(1.179 \pm 0.009) \times 10^{10}$  fis/ml is in excellent agreement with the INEL result of  $(1.176 \pm 0.026) \times 10^{10}$  fis/ml. It should be emphasized that these two values are independent of each other. The only point in common is the fact that fission chambers are used in the basic fission rate measurements. Thus an excellent check is provided on the presence of any significant

**TABLE A-II**  
**NUMBER OF FISSIONS FOR LASL SAMPLE**  
**FROM INEL ANALYSIS**

<u>Isotope</u>	<u>Number of Fissions (<math>10^{10}/ml</math>)<sup>a</sup></u>	
	<u>ILRR Yields</u>	<u>Meek and Rider Yields</u>
<sup>95</sup> Zr-724	1.176 ± 0.020	1.186 ± 0.023
-756	1.165 ± 0.020	1.175 ± 0.023
<sup>108</sup> Ru	1.189 ± 0.019	1.141 ± 0.022
<sup>140</sup> Ba- <sup>140</sup> La	1.171 ± 0.020	1.158 ± 0.020
Average	1.176 ± 0.010	1.164 ± 0.011
	1.176 ± 0.026 <sup>b</sup>	1.164 ± 0.022 <sup>b</sup>

<sup>a</sup>See text for discussion of error contributions.

<sup>b</sup>Uncertainties in fission yields are added in quadrature to that of the average; see text.

**TABLE A-III**  
**UNCERTAINTIES ASSIGNED IN INEL MEASUREMENTS**

<u>Isotope</u>	<u>Uncertainty (%)</u>					
	<u>Counting<sup>a</sup></u>	<u>Half-Life Terms</u>	<u>Branching Ratio</u>	<u>Detector Efficiency</u>	<u>Fission Yield</u>	
					<u>ILRR</u>	<u>Meek and Rider</u>
<sup>95</sup> Zr	0.5	0.5	1.0	1.5	2.0	1.4
<sup>108</sup> Ru	0.4	0.2	1.1	1.5	2.0	2.0
<sup>140</sup> Ba- <sup>140</sup> La	0.8	0.1	0.1	1.5	2.0	1.4

<sup>a</sup>This contribution includes errors in peak areas and the consistency of the measurements.

**TABLE A-IV**  
**NUMBER OF FISSIONS FROM**  
**LASL ANALYSIS**  
**(Results from Ref. 10.)**

Isotope	Fissions (10 <sup>10</sup> /ml)	Precision (%)
<sup>99</sup> Mo	1.180	0.19
<sup>140</sup> Ba	1.171	0.46
Average	1.179 ± 0.003	
	1.179 ± 0.009 <sup>a</sup>	

<sup>a</sup>Uncertainty includes contribution of 0.72% from K-factor as discussed in Sec. III.D of Ref. 1.

systematic errors that have not been taken into account.

One minor restriction on the above comparison should be noted. The INEL-LASL agreement above is for the LASL radiochemical analyses of <sup>99</sup>Mo and <sup>140</sup>Ba. In association with the decay heat measurements, the LASL determination of the number of fissions is based on both the radiochemical analyses for these isotopes and gamma-ray spectral analyses for several isotopes. Any systematic difference between these two types of analyses would confuse the question of agreement between the LASL and INEL results. In fact, the values in Table I of Ref. 1 do give a slightly lower, by 0.3%, value from the radiochemical analyses than for the average values. However, even if this bias really exists, the INEL and LASL analyses still will be in excellent agreement.

From the sample sent by LASL to ORNL, the ORNL group<sup>2</sup> made two sources, one containing 1.00% of sample and the other containing 5.00%. These samples were counted with the same Ge(Li) gamma-ray detectors as used to determine the fissions for the ORNL decay heat measurements. Two calibration methods were used. The first, called the absolute method, involves determining the absolute gamma-ray emission rates and using the gamma-ray branching ratios and isotopic fission yields to determine the number of fissions. This is the same as the INEL method except different isotopes were used. The second calibration method is the K-factor

technique where a fission chamber is used to determine the number of fissions in the sample. The gamma-ray counting rates are determined for the same, or an identical, sample. Then only relative gamma-ray counting rates are needed for the unknown sample. This is, in part, similar to the LASL method.

The values of the gamma-ray branching ratios and fission yields used by ORNL in the "absolute" methods have been compared with various evaluations. The agreement is good; in the worst cases, the variations are about 1%.

After ORNL had completed their counting, the source containing 5.00% of their sample was sent to the INEL. If the sample preparations were all correct, the relative activity of the original INEL sample to that of this sample should be 20.00. This ratio, as measured at the INEL, was 19.97 ± 0.14. This indicates that the preparations were satisfactory.

The results of the ORNL measurements for the number of fissions in the LASL sample are given in Table A-V for three isotopes and the two methods described above. The uncertainties in the six individual values are quoted in Ref. 2 as 2.5%. We compute the uncertainty in the final average to be 1.5%, but this depends on the magnitude of the separate components of the individual errors and

**TABLE A-V**  
**NUMBER OF FISSIONS FROM**  
**ORNL ANALYSIS**  
**(Results from Ref. 2.)**

Isotope	Fissions (10 <sup>10</sup> /ml) <sup>a</sup>	
	Absolute Method	K-Factor Method (20 cm)
<sup>99</sup> Mo	1.172	1.193
<sup>132</sup> Te	1.178	1.197
<sup>97</sup> Zr- <sup>97</sup> Nb	1.176	1.190
Average	1.175	1.193
Average	1.184	

<sup>a</sup>Uncertainty in each of the six measured values is assigned as 2.5%.

the assumptions made about their correlations. With this error, the final ORNL value would be  $(1.184 \pm 0.018) \times 10^{10}$  fis/ml. This is in good agreement with the LASL and INEL values of  $(1.179 \pm 0.009) \times 10^{10}$  and  $(1.176 \pm 0.026) \times 10^{10}$  fis/ml, respectively. Although one may question whether these uncertainties are all comparable (e.g., the LASL value is three times more accurate than the INEL value), the agreement to better than 1% in the values is very satisfying and should help place the associated decay heat measurements on a firm basis.

#### APPENDIX REFERENCES

1. J. L. Yarnell and P. J. Bendt, "Decay Heat from Products of  $^{235}\text{U}$  Thermal Fission by Fast-Response Boil-Off Calorimetry," Los Alamos Scientific Laboratory report LA-NUREG-6713 (1977).
2. J. K. Dickens, Oak Ridge National Laboratory, personal communication, April 1977.
3. R. C. Greenwood, R. G. Helmer, J. W. Rogers, N. D. Dudey, R. J. Popek, L. S. Kellogg, and W. H. Zimmer, "Nonfission Reaction Rate Measurements," Nucl. Tech. **25**, 274 (1975).
4. R. J. Gehrke, R. G. Helmer, and R. C. Greenwood, Idaho National Engineering Laboratory, to be published.
5. R. G. Helmer and R. C. Greenwood, "LMFBR Reaction Rate and Dosimetry 11th Progress Report," to be published as HEDL-TME report.
6. R. G. Helmer and R. C. Greenwood, "Evaluated Decay Scheme Data," Nucl. Tech. **25**, 258 (1975).
7. R. G. Helmer and R. C. Greenwood, "LMFBR Reaction Rate and Dosimetry 9th Progress Report," HEDL-TME 74-45 (W. N. McElroy, Ed.), P. ANC-49 (1974).
8. D. M. Gilliam, "Memorandum for ILRR Participants," personal communication, July 1976.
9. N. E. Meek and B. F. Rider, "Recommended Yields for ENDF/B (June 1976)," as quoted in Ref. 8 above.
10. G. W. Knobeloch, Los Alamos Scientific Laboratory, personal communication, November 1976.